

Impact of measured spectrum variation on solar photovoltaic efficiencies worldwide

Geoffrey S. Kinsey¹, Nicholas C. Riedel-Lyngskær², Miguel Alonso-Abella³, Matthew Boyd⁴, Marília Braga⁵, Shou Chunhui⁶, Raul R. Cordero⁷, Benjamin C. Duck⁸, Christopher J. Fell⁸, Sarah Feron⁷, George Georghio⁹, Nicholas Habryl¹⁰, Jim J. John¹¹, Nipon Ketjoy¹², Gabriel López¹³, Atse Louwen¹⁴, Loyiso Maweza¹⁵, Takashi Minemoto¹⁶, Ankit Mittal¹⁷, Cécile Molto¹⁰, Guilherme Neves¹⁸, Gustavo Nofuentes Garrido¹⁹, Matthew Norton⁹, Basant R. Paudyal²⁰, Enio Bueno Pereira¹⁸, Yves Poissant²¹, Lawrence Pratt¹⁵, Shen Qu⁶, Thomas Reindl²², Marcus Rennhofer¹⁷, Carlos D. Rodríguez-Gallegos²², Ricardo Rütther⁵, Wilfried van Sark²³, Miguel A. Sevillano-Bendezú²⁴, Hubert Seigneur¹⁰, Jorge A. Tejero¹⁹, Marios Theristis²⁵, Jan A. Töflinger²⁴, Carolin Ulbrich²⁶, Waldeir Amaral Vilela¹⁸, Xiangao Xia²⁷, Márcia A. Yamasoe²⁸

Abstract

In photovoltaic power ratings, a single solar spectrum, AM1.5, is the de facto standard for record laboratory efficiencies, commercial module specifications, and performance ratios of solar power plants. More detailed energy analysis that accounts for local spectral irradiance, along with temperature and broadband irradiance, reduces forecast errors to expand the grid utility of solar energy. Here, ground-level measurements of spectral irradiance collected worldwide have been pooled to provide a sampling of geographic, seasonal, and diurnal variation. Applied to nine solar cell types, the resulting divergence in solar cell efficiencies illustrates that a single spectrum is insufficient for comparisons of cells with different spectral responses. Cells with two or more junctions tend to have efficiencies below that under the standard spectrum. Silicon exhibits the least spectral sensitivity: relative weekly site variation ranges from 1% in Lima, Peru to 14% in Edmonton, Canada, with a mean of 4%.

Introduction

To anyone who has ever watched a sunset or gazed upon a deep blue sky, the idea of variation in the spectrum of sunlight is hardly surprising. Yet consideration of spectrum variation has often played a minor role in both solar photovoltaic development and operations. When comparing solar photovoltaic (PV) efficiencies, assessing output of solar power plants, and evaluating warranty claims, the power rating is generally used, for which a single standard spectrum (AM1.5, Appendix A) is the reference. Reliance on the single standard spectrum has its advantages, including providing continuity over the years and consistency across academia and industry, but neglect of spectrum variation adds to uncertainty in predictions of solar energy generation^{1–10}. For variable sources such as solar (and wind) to displace conventional sources and become the backbone of future energy supply, electrical grids must be buffered against impacts from their limited availability and potential underperformance¹¹. Reduction in forecast errors¹² complements other tools, such as battery storage, which brings increasing marginal costs as variable sources become a larger fraction of the supply¹³.

Three factors determine the efficiency of a solar photovoltaic cell: temperature, irradiance, and the spectrum of irradiance (the spectral irradiance)¹⁴. Historically, application of the first two factors has been distinct from that of the third. Temperature and (broadband) irradiance are routinely measured at solar installations and applied to forecasts of the grid availability of solar energy. Measurements of the third factor, spectral irradiance, are comparatively sparse, conducted sporadically and at limited locations worldwide. The power output of solar modules is rated using the single spectrum and residential, commercial, and utility-scale PV systems are designed accordingly. For example, to determine if a solar power plant is performing to its contractual obligations, a key metric is the “performance ratio”¹⁵. This is calculated as the energy generated in a given time period divided by the broadband irradiance and the efficiency under the AM1.5 spectrum: variation in the spectrum is neglected.

The AM1.5 reference spectrum was standardized in 1982¹⁶ as an analog to the single spectrum used in space (AM0). Given the variability in terrestrial atmospheric conditions, concerns with over-reliance on it followed soon after^{3,9,17,18}. Yet the information gap between spectral irradiance and temperature & broadband irradiance called out specifically in [3] has persisted. Growth of the solar industry has led to temperature and broadband irradiance variation requirements being codified into international power ratings¹⁹, data sheets²⁰, and warranty terms²¹. In applications where use of the power rating (rather than more detailed energy analyses)

predominates, the impact of spectral irradiance variation has often been treated as a secondary concern or neglected²². The current international standard for solar module power rating defines four temperatures and four broadband irradiances, but only one spectrum²³. The persistence of the gap has been due partly to the perceived expense in obtaining spectral irradiance measurements, as well as a legacy assumption that the impact on silicon, solar energy’s workhorse material, is negligible. Increasing deployments of silicon PV lead to relatively small factors growing in absolute terms, so it may be worth revisiting these assumptions.

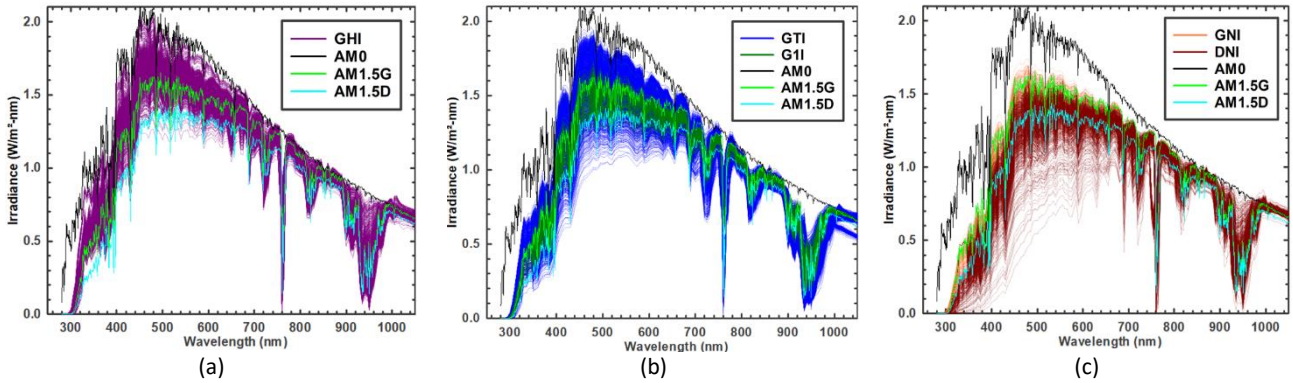


Figure 1. Spectral irradiance measured at the sites in Table 1: (a) global horizontal irradiance (GHI) (b) global tilt irradiance (GTI) and global one-axis irradiance (G1I); (c) global normal irradiance (GNI) and direct normal irradiance (DNI). Each line is a weekly sum of spectral irradiance sampled at 10-minute intervals (except for Chajnantor, CHL: 60-minute intervals). The spectrum for global horizontal irradiance (GHI), measured with sensors pointed upward at the dome of the sky is, not surprisingly, the “bluest”. As the degree of solar tracking increases, the sensors begin to follow the sun to the horizons; the irradiance passes through a larger air mass and shifts away from “blue” to the “red” and infrared; visible wavelengths (400-700 nm) are diminished. The spectra are normalized at either 880 nm or 1050 nm; AM1.5 values are substituted outside the measurement ranges. Standard spectra (AM0²⁴, AM1.5G, AM1.5D²⁵) are shown for reference.

The solar market approaches €200 billion annually²⁶ and impending rapid climate change makes every kWh of renewable energy more precious. Variation of mere tenths of a percent already imply billions of euros gained or lost over the decades of operation - before any cost of carbon is included²⁷. For a single 100-MW PV plant that displaces fossil-fuel generation at 1500 kWh/kW, any 2% variation in generation is equivalent to about €150,000 in annual revenue and ~1,500 tons of avoided CO₂, or nine one-way flights between New York and Paris per year²⁸. As of 2021, the world has installed PV capacity equivalent to eight thousand such plants²⁹. Public and private sectors are pivoting to decarbonization of the global economy, so maximizing the extent to which solar energy supports the future grid depends on minimizing uncertainty in the availability of solar assets. If solar is to provide 22% of the world’s electricity by 2050³⁰, 2% of the implied 9,000 TWh/yr would exceed the present annual generation of Poland³¹.

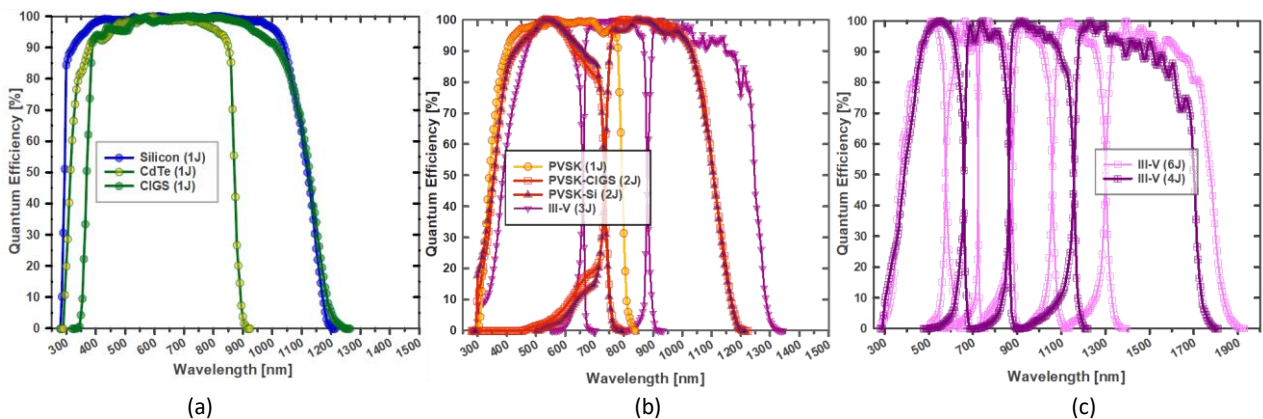


Figure 2. Solar cell quantum efficiencies digitized at 5-nm intervals from the Solar Cell Efficiency Tables: (a) silicon (Si), cadmium telluride (CdTe), and copper indium gallium selenide (CIGS); (b) perovskite (PVSK), perovskite-CIGS tandem (PVSK-CIGS), perovskite-silicon tandem (PVSK-Si), and a three-junction III-V; (c) four-, and six-junction III-Vs.

Meanwhile, successive increments in the efficiency of silicon PV over the last decade have depleted the reserve of remaining options. As recently as 2017³², more than half of worldwide PV production was still a traditional aluminum/back-surface-field (Al-BSF) design on multicrystalline wafers and the industry could look forward to continuing efficiency increases from the transition to PERC designs (~9% relative) on monocrystalline silicon

(~5% relative). For further improvements, the industry must now turn to smaller increments from more capital-intensive options such as tunnel-oxide contacts on n-type wafers (~3% relative) or heterojunction cells (~4% relative). With the efficiency of silicon beginning to plateau, the international PV industry roadmap now anticipates relying on tandem solar cells for some future growth as early as 2023³³. The extent to which tandem designs could deliver not just higher rated power, but also lower cost of energy in operation, depends in part on their sensitivity to spectrum variation. As designs using novel materials have proliferated³⁴, evidence for a need to incorporate spectrum variation^{4-6,10,35-66} in the power ratings has grown harder to ignore. The work presented here dovetails with a larger effort within the PV sector to expand beyond instantaneous power ratings (kW) to more fully consider energy generation over time (kWh)⁶⁷. In 2018, the international standard for power rating was complemented with energy ratings for six climatic zones^{68,69} that give irradiance values in twenty-eight wavelength bands (Appendix B). However, given the limited measured spectral irradiance data available, previous studies on its impact have had to rely on relatively small data sets, or synthetic spectra^{5,28,48,70}.

Measured spectral irradiance

A coalition of solar researchers has pooled their data from sites in Africa, Asia, Australia, Europe, and the Americas that span a range of latitudes, elevations, atmospheric conditions, and orientations (Figure 1). Spectral irradiance is typically measured by spectroradiometers, instruments which employ optical diffraction to measure irradiance across a series of narrow wavelength ranges. A given diffractive optic and its detector can sample only a limited wavelength range, so spectroradiometers for PV applications often measure total wavelength ranges of around 300-1100 nm or 900-1700 nm⁷¹ (Table 1). A pair of spectroradiometers spanning 300-1700 nm measures about 97% of the power in the extraterrestrial (AM0) spectrum²⁴. An alternative is to use a “solar spectral irradiance meter” that takes measured irradiance at a relatively small number of specific wavelengths as inputs to a model to reconstruct the full spectrum^{72,73}. This is the instrument used for locations in Table 1 where the wavelength range is described as 280-4000 nm.

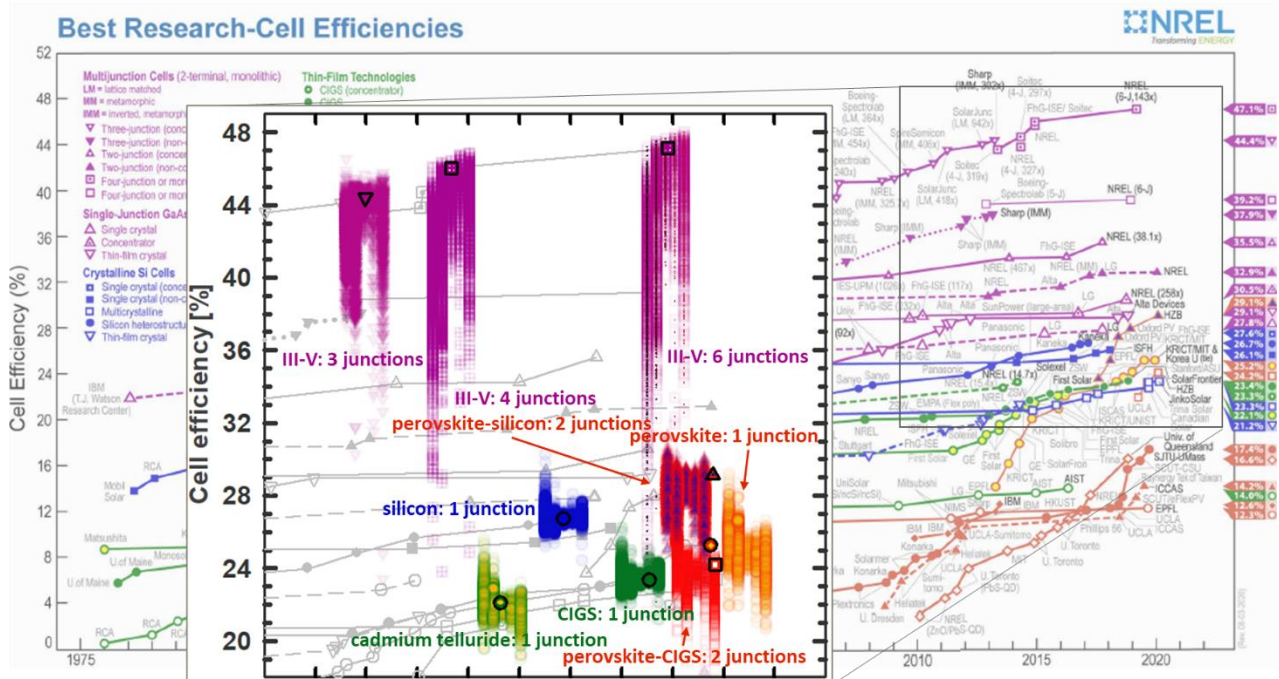


Figure 3. Efficiencies under measured spectral irradiance, compared against the values under Standard Test Conditions (symbols with black border). Symbols are arranged in order of increasing sun tracking: GHI, GTI, G1I, GNI, DNI. Lateral positions are adjusted to improve visibility. Each data point is a weekly sum from spectral irradiance sampled at 10-minute intervals (except for Chajnantor, CHL: 60-minute intervals). Best Research-Cell Efficiency chart courtesy of NREL.

In parallel with direct measurement of ground-level spectral irradiance is the formulation of synthetic spectra. Synthetic spectra are formed by applying physical models using inputs of atmospheric properties that, in turn, are derived from radiometry over select wavelength ranges (Appendix G)^{8,74-78}. Limited ground-level measurement of the atmospheric parameters is augmented with satellite telemetry to produce synthetic spectra over extended geographic areas^{77,78}. While synthetic spectra have demonstrated the ability to predict

solar energy generation under a narrow set of field conditions^{79–81}, ground-level measurements such as those provided here are needed to fine-tune the models and verify that the synthetic spectra remain accurate across the broader range of atmospheric conditions under which solar energy is now generated worldwide. Synthetic spectra have previously been applied to analysis of the nine cell types in [28]. A pattern of offsets between results from synthetic^{77,78} and measured spectral irradiance is in Appendix G.

Spectral irradiance sensors are mounted in orientations with varying degrees of solar tracking (Figure 1). Measurement of spectral irradiance has applications beyond solar PV, including monitoring of pollution⁸² and the radiative forcing arising from water vapor and other greenhouse gases^{83,84}. As such, the most common orientation is horizontal, with the sensor exposed to the “global” spectrum arriving from the full hemisphere of the sky (global horizontal irradiance, “GHI”). For solar energy applications, preferred orientations are those that match the “plane of array” in which solar modules are mounted. The most common mounting orientation for PV modules is either a fixed tilt (global tilted irradiance, or “GTI”) or one-axis tracking (global one-axis irradiance, “G1I”). Two-axis tracking keeps the surface perpendicular (normal) to the sun’s rays and global normal irradiance (“GNI”) is obtained. Finally, to capture irradiance coming only directly from the vicinity of the solar disc, two-axis tracking is combined with collimators that exclude scattered sunlight for measurement of direct normal irradiance (“DNI”).

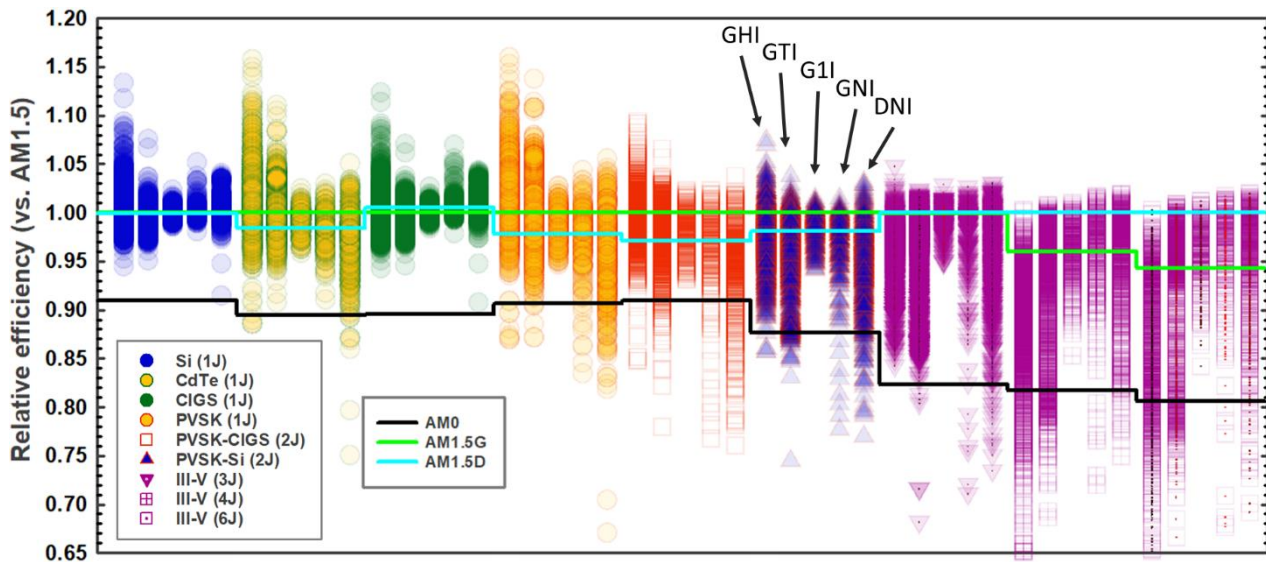


Figure 4. Relative efficiency as a function of cell type and number of junctions: silicon (Si), cadmium telluride (CdTe), CIGS, perovskite (PVSK), perovskite-CIGS tandem (PVSK-CIGS), perovskite-silicon tandem (PVSK-Si), and three-, four- and six-junction III-V multijunctions. For each cell type, data is grouped by orientation: from left to right, GHI, GTI, G1I, GNI, DNI. Lines indicate the relative efficiency of each type under the three standard solar spectra. AM0 is the standard spectrum outside Earth’s atmosphere²⁴. Each data point is a weekly sum from spectral irradiance sampled at 10-minute intervals (except for Chajnantor, CHL: 60-minute intervals).

Analysis

The influence of spectral variation on nine solar cell types is evaluated using their current-best characteristics (Appendix E), as given in the Solar Cell Efficiency Tables⁸⁵ and NREL’s Best Research-Cell Efficiency Chart³⁴. Four single-junction cells (silicon⁸⁶, cadmium telluride⁸⁷, CIGS⁸⁵, and perovskite⁸⁸) are considered, along with five two-terminal multijunctions (perovskite-CIGS⁸⁹, perovskite-silicon⁸⁹, and three-, four- and six- junction III-Vs^{85,87,90}). Multijunctions convert solar energy using two or more semiconductor junctions. Stacking the junctions increases the cell voltage while splitting the conversion of sunlight into current from each junction. The two-terminal configuration implies a series connection, so the overall device current is limited by whichever junction is producing the least current. As a result, two-terminal multijunctions have more sensitivity to spectrum variation. In a solar module sunlight must pass through solar glass and encapsulants before reaching the solar cells, but the high transmission through these materials⁹¹ makes the bare-cell spectral responses of Figure 2 useful proxies for commercial PV modules.

Efficiencies from the measured spectra are shown in Figure 3, against a backdrop of the confirmed values under AM1.5G (AM1.5D, for III-V multijunctions). The corresponding relative efficiencies are shown in Figure 4. Cells with a single junction (Si, CdTe, CIGS, and PVSK) demonstrate efficiencies clustered about their efficiency under the AM1.5 standard spectrum. As the number of junctions increases, the degree of spectrum sensitivity increases, and the relative efficiencies in Figure 4 drop. For cells with two or more junctions, the performance under AM1.5, rather than being an average value (as with the single-junction cells), tends to be more of an upper bound of the performance seen under measured spectra. Energy generation will therefore be lower than for a single-junction cell with the same power rating.

Series-connected tandems and multijunctions are tuned (by varying the thickness and/or composition of the individual junctions) to optimize current matching of each junction under a given target spectrum. Cells engineered to perform best under AM1.5, therefore, may have been de-tuned from optimum performance in operating conditions. Rating solar efficiency under a single spectrum is a bit like designing a vehicle solely for highway (not city) driving⁹²: it is unlikely to lead to all-around higher performance. Re-designing solar cells for the range of spectral conditions in operation^{93,94} will require different thicknesses and (where possible) material compositions. The practice of tuning for operation under AM1.5, alone, may therefore have an adverse effect on the development of these serially-connected tandems and multijunctions. As shown in Appendix L, Lima and Singapore are coastal sites with particularly high (and stable) levels of humidity where the efficiencies of the more spectrum-sensitive designs converge on that of silicon.

Consistent with the existing power ratings that contain several temperature and broadband irradiances¹⁹, power rating under more than one spectrum would enable interpolation and extrapolation to other atmospheric conditions, providing some of the benefits of the more complex energy analyses. Figure 4 suggests that AM0, the standard spectrum in space applications²⁴, is one example that could be re-purposed to bracket much of the terrestrial spectrum variation²⁸. Fortunately, characterization under two spectra does not require two measurements: if the spectral response of a cell is known, efficiency under a single condition can be translated to that under a second condition using a calculation known as “spectral mismatch correction”⁹⁵.

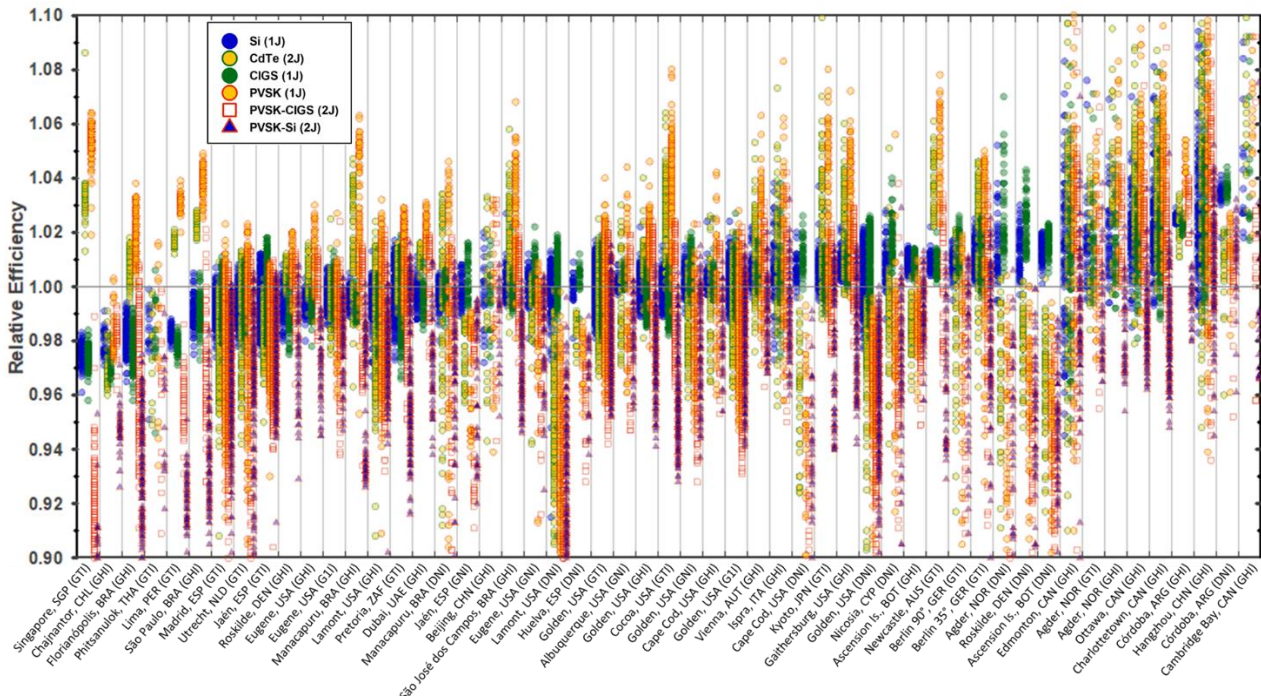


Figure 5. Relative efficiency vs. location and orientation for cells with one or two junctions. Data is sorted by increasing median efficiency of silicon. Location names are approximate. Each data point is a weekly sum from spectral irradiance sampled at 10-minute intervals (except for Chajnantor: 60-minute intervals).

Cells with a wider spectral response (Figure 2) are more tolerant to the increased spectral variation that arises from sun tracking. In Appendix H, increasing the sun tracking is seen to benefit single-junction cells with a wider spectral response (silicon, CIGS), but is a detriment to cells with a narrower spectral response (cadmium

telluride, perovskites), confirming predictions from synthetic spectra^{28,48,49}. For cells with more than one junction, the correlation is more complex, as losses due to current mismatch between the junctions trade against the wider spectral response of the overall stack.

The fuel transportation costs for solar energy are tough to beat. Inherent variability in the supply, however, brings challenges; concerns about its availability limit the grid penetration of solar PV⁹⁶. Of prime importance to solar array owners, project developers, power plant managers, and grid operators is the real-time variation for their specific location and mounting orientation. Site-specific relative efficiency values are given in Figure 5, ranked in order of increasing median efficiency for silicon (absolute efficiencies, Appendix F). The performance of CIGS, with a similar spectral response, tracks the increase with silicon; all other efficiencies diverge. The AM1.5 spectrum was conceived for use with silicon cells in North America, so it is a tribute to its accuracy that most sites in North America exhibit the least offset from the standard. As might be expected, sites at higher latitudes (with the largest excursions in sun angle and air mass) see the largest variation, but there are notable exceptions (Appendix I). Similar variation is also seen in Hangzhou (30° latitude); this is likely driven by light scattering effects of aerosols, as it is a city of over ten million inhabitants that currently ranks in the lower tier for air quality in China⁹⁷. Spectral variation from urban aerosols compounds attenuation of the broadband irradiance and therefore shifts the calculation of where best to site PV generation to minimize transmission losses⁹⁸. Both long-term oscillations in local aerosol levels (global dimming & brightening⁹⁹) and accelerating climate change diminish the predictive power of forecasts that depend on archived spectral irradiance values.

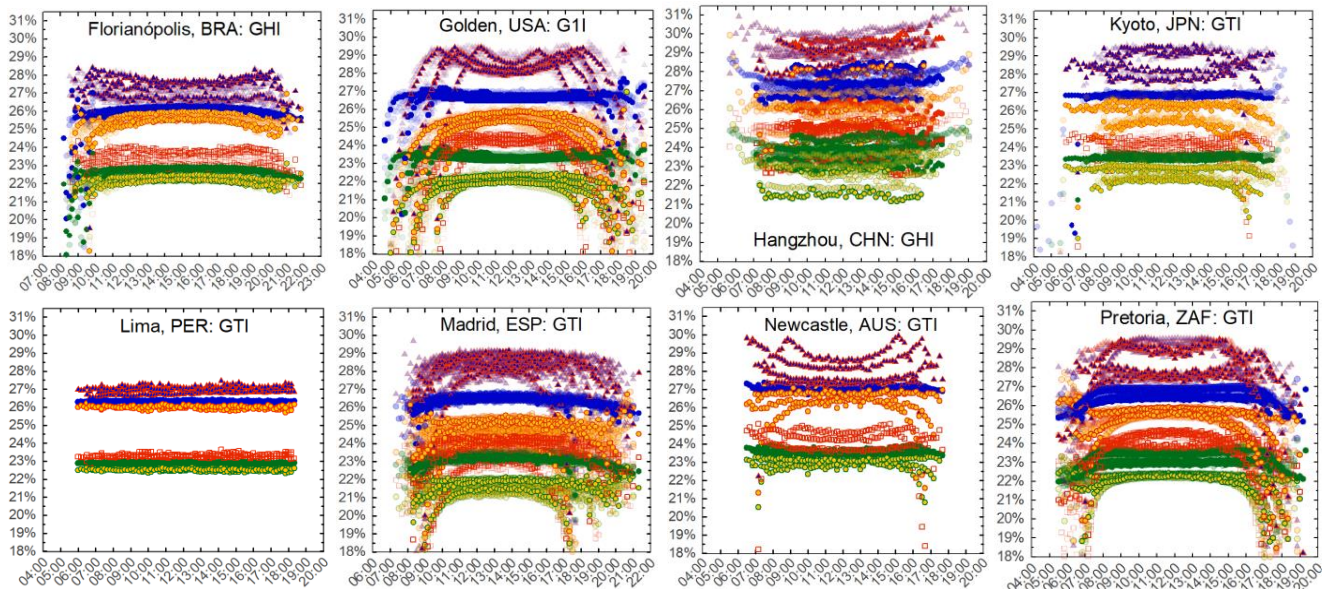


Figure 6. Sample seasonal and diurnal efficiency variations for cells with one or two junctions. Seasonal changes are delineated using one month of data for March, June, September, and December. Where available, data from additional years is semi-transparent in the background. Each data point is a sum of data at a 10-minute interval for a month. Results for all locations are shown in Appendix K. (Refer to Figure 5 for a legend.)

Sample seasonal and diurnal variations are shown in Figure 6. Figures for the remaining sites, and for annual variation, are included in Appendix K. For power plant and grid operators, unanticipated fluctuations in generation, be it losses or gains, can be costly. To meet contractual obligations and grid demand, forecasts for the month, day, and hour ahead are often stipulated; gaps between the expected and actual output result in power surpluses or deficits that can disrupt grid stability. Operators of solar power plants therefore employ meteorological (“met”) stations to monitor temperature, wind, and plane-of-array (broadband) irradiance. In larger plants, there are often multiple broadband irradiance instruments¹⁰⁰. In the absence of spectral irradiance monitoring, however, the variation of Figure 6 is necessarily confounded with other uncertainties: module and inverter degradation, soiling, cable corrosion, etc.¹⁰¹ Unexplained losses of a few percent can trigger costly contract disputes or warranty claims. Conversely, unplanned surpluses lead to transmission line congestion and curtailment of generation, due to cabling and power electronics that are undersized, or grid operators unprepared to receive the surge of excess power. Implementing site monitoring procedures for spectral

irradiance in line with those established for temperature and broadband irradiance will curb these losses and allow for larger allocations of solar energy assets to displace conventional sources.

So long as the cost of electricity storage exceeds that of renewable generation¹⁰² and efforts to “electrify everything”¹⁰³ to blunt impending climate disruptions gain traction, solar power will be increasingly most valuable at the very times¹⁰⁴ it is least available. An (extreme) example is the winter storm that hit the Texas, USA grid in February 2021. Temperatures below freezing caused loss of generation from (insufficiently weatherized) sources that depend on moving parts and the flow of liquids: natural gas, coal, nuclear, and wind. Winter is not usually considered solar energy’s best season, but as other generators dropped offline and electricity prices spiked by factors of more than five¹⁰⁵, solar generation was the only source to deliver increased output¹⁰⁶. It can be hard to predict exactly when solar energy will be most valuable, so efforts to both quantify and minimize daily and seasonal spectral variation losses are needed to maximize the projected availability of solar energy in grid operations. As solar assets come to take up larger portions of grid capacity, generation during the “shoulder” periods seen in seasonal and diurnal output (Appendix K & L) will increase in value. Silicon produces the most stable output under seasonal spectrum variation: its weekly site-level variation ranges from 1% to 14%, with a mean of 4% (Table 1 & Appendix J). Though this is the least of the cells evaluated, the mean remains equivalent to more than 10° C of temperature variation, or five years of module degradation¹⁰⁷. Where AM1.5 substitutions were made due to limited measurement range (Appendix D), these are underestimates.

Conclusion

The variation in measured spectral irradiance data reveals patterns in the impact on solar photovoltaic performance worldwide. The magnitude of the cell efficiency variation indicates that the convention of rating PV power under a single spectrum is insufficient for comparison of different cell types. Spectrum sensitivity increases with the number of junctions and efficiency correspondingly declines. For tandems and multijunctions, efficiency under the standard spectrum is closer to a maximum than a representative value: the practice of designing for AM1.5 may be reducing the potential for energy generation in operation. Having two spectra in the power rating (AM1.5 and AM0, for example) would serve to bracket the operating performance range, better inform solar cell development, and accelerate deployment. Silicon is less sensitive than other candidate materials, but the declining options for further improvements in its efficiency, combined with the sheer scale of future PV deployments, enhance the value of spectrum variation in both relative and absolute terms. Solar energy can provide a larger percentage of grid electricity if forecast errors are reduced via expanded monitoring, in line with that of temperature and broadband irradiance.

Table 1. Relative efficiency variation using weekly sums of spectral irradiance at the sensor locations (source shown in brackets). The orientations are global horizontal irradiance (GHI), global tilted irradiance (GTI), global, 1-axis tracking irradiance (G1I), global normal irradiance (GNI), and direct normal irradiance (DNI). Spectral irradiance is sampled at 10-minute intervals (except at Chajnantor: 60-minute) and summed over each week for each data point. Location names are approximate. The Berlin site has sensors tilted at local latitude (35°) and vertically (90°). Numbers in brackets indicate the contributing authors; the source for superscript numbers is given in the references.

Cell type (number of junctions):		Silicon (1)	CdTe (1)	CIGS (1)	PVSK (1)	PVSK-CIGS (2)	PVSK-Si (2)	III-V (3)	III-V (4)	III-V (6)		
Standard absolute efficiencies:		AM0	24.3%	19.8%	20.9%	22.9%	22.0%	25.6%	36.6%	37.6%	38.0%	
		AML5G	26.7%	22.1%	23.4%	25.2%	24.2%	29.2%	44.4%	44.2%	44.4%	
		AML5D	26.7%	21.8%	23.5%	24.6%	23.5%	28.6%	44.4%	46.0%	47.1%	
Location & orientation [source]	Range [nm]	Years	Relative efficiencies ($\frac{\eta - \eta_{src}}{\eta_{src}}$):									
Agder, NOR [20]	GHI	280-4000	2020	-1% to 7%	0% to 11%	-1% to 6%	0% to 12%	-1% to 4%	-5% to 2%	-15% to 1%	-35% to -6%	-46% to -6%
Agder, NOR [20]	GTI	280-4000	2020	-1% to 8%	-2% to 11%	-1% to 7%	-3% to 11%	-4% to 7%	-4% to 4%	-7% to 2%	-37% to 1%	-48% to 1%
Agder, NOR [20]	DNI	280-4000	2020	-1% to 5%	-9% to 1%	1% to 7%	-16% to 0%	-23% to 0%	-22% to 1%	-29% to 3%	-28% to 2%	-40% to 2%
Albuquerque, USA [108]	GNI	350-1700	2015	0% to 1%	-3% to 3%	0% to 1%	-4% to 4%	-5% to 2%	-5% to 0%	-8% to 1%	-13% to 1%	-14% to 1%
Ascension Island, BOT [109]	GHI	350-1320	2016-2017	0% to 1%	-8% to 0%	0% to 1%	-13% to 2%	-18% to 1%	-17% to 1%	-20% to 2%	-11% to -3%	-11% to -4%
Ascension Island, BOT [109]	DNI	350-1320	2016-2017	0% to 2%	-8% to 0%	0% to 2%	-12% to -1%	-16% to -2%	-15% to -1%	-17% to 1%	-16% to -1%	-20% to -1%
Beijing, CHN [27]	GHI	280-4000	2019	-3% to 2%	-6% to 3%	-3% to 2%	-6% to 3%	-6% to 3%	-5% to 1%	-5% to 0%	-12% to -3%	-15% to -3%
Berlin 35°, GER [26]	GTI	300-1700	2019-2020	0% to 2%	-4% to 5%	0% to 3%	-7% to 5%	-11% to 4%	-10% to 2%	-12% to 2%	-28% to 0%	-31% to 0%
Berlin 90°, GER [26]	GTI	300-1700	2020	0% to 2%	-8% to 0%	0% to 3%	-13% to 2%	-18% to 1%	-17% to 1%	-20% to 2%	-19% to 0%	-22% to 0%
Cambridge Bay, CAN [21]	GHI	280-4000	2019	2% to 13%	3% to 10%	2% to 12%	-1% to 11%	-4% to 9%	-3% to 7%	-9% to 1%	-44% to -13%	-55% to -18%
Cape Cod, USA [110]	GHI	350-1700	2012-2013	0% to 2%	-4% to 3%	-1% to 3%	-4% to 4%	-5% to 2%	-5% to 1%	-6% to 1%	-17% to -3%	-22% to -4%
Cape Cod, USA [110]	DNI	350-1700	2012-2013	0% to 2%	-8% to 0%	0% to 3%	-11% to 1%	-15% to -2%	-14% to -1%	-16% to 1%	-14% to 0%	-17% to 1%
Chajnantor, CHL [7]	GHI	290-1800	2016-2017	-3% to -1%	-4% to -1%	-4% to -2%	-3% to 0%	-4% to -1%	-7% to -3%	-4% to -7%	-12% to -4%	-14% to -10%
Charlottetown, CAN [21]	GHI	280-4000	2018-2021	-1% to 8%	0% to 11%	-1% to 8%	0% to 12%	-2% to 9%	-5% to 5%	-12% to 1%	-37% to -8%	-48% to -9%
Cocoa, USA [10]	GTI	350-1600	2018-2021	-1% to 2%	0% to 6%	-2% to 1%	-1% to 8%	-4% to 2%	-7% to 0%	-17% to 0%	-30% to -8%	-30% to -7%
Córdoba, ARG [111]	GHI	350-1340	2018-2019	2% to 3%	1% to 3%	2% to 3%	3% to 5%	2% to 4%	-2% to 2%	-6% to -3%	-25% to -21%	-23% to -20%
Córdoba, ARG [111]	DNI	350-1340	2018-2019	2% to 4%	-4% to 2%	2% to 4%	-4% to 3%	-5% to 2%	-4% to 3%	-3% to 3%	-20% to -6%	-18% to -4%
Dubai, UAE [11]	GHI	300-1050	2020-2021	-1% to 1%	0% to 2%	-2% to 1%	1% to 3%	-3% to 2%	-6% to 1%	-7% to 2%	-12% to -4%	-11% to -5%
Edmonton, CAN [21]	GHI	280-4000	2018-2020	-6% to 8%	-10% to 11%	-6% to 8%	-12% to 10%	-13% to 9%	-12% to 7%	-11% to 5%	-35% to -4%	-45% to -4%
Eugene, USA [112]	GHI	350-1050	2020-2021	-2% to 0%	-1% to 2%	-2% to 0%	-1% to 3%	-2% to 1%	-6% to -1%	-5% to 0%	-11% to -3%	-10% to -4%
Eugene, USA [112]	G1I	300-1050	2018-2020	-1% to 1%	-3% to 3%	-2% to 1%	-4% to 3%	-6% to 2%	-5% to 0%	-5% to 1%	-9% to 1%	-7% to 1%
Eugene, USA [112]	GNI	300-1050	2020-2021	-2% to 1%	-6% to 1%	-2% to 2%	-9% to 1%	-12% to 0%	-11% to 0%	-11% to 2%	-9% to 1%	-11% to 1%
Florianópolis, BRA [5]	GHI	295-1100	2018-2020	-4% to -1%	-1% to 2%	-4% to -1%	0% to 4%	-9% to 1%	-12% to -2%	-13% to -2%	-19% to -6%	-20% to -6%
Gaithersburg, USA [113]	GHI	335-1650	2016-2018	0% to 2%	0% to 6%	0% to 2%	0% to 7%	-2% to 3%	-6% to 1%	-14% to 1%	-30% to -6%	-32% to -6%
Golden, USA [114]	GHI	300-1000 280-4000	2012-2015 2021	-1% to 2%	-2% to 4%	-2% to 2%	-2% to 5%	-2% to 2%	-6% to 1%	-6% to 0%	-18% to -4%	-23% to -4%
Golden, USA [114]	GTI	350-1050	2016-2021	-2% to 2%	-3% to 3%	-2% to 2%	-4% to 4%	-6% to 2%	-5% to 1%	-5% to 2%	-9% to 0%	-7% to -1%
Golden, USA [114]	G1I	350-1650	2016-2021	-1% to 2%	-4% to 2%	-1% to 3%	-5% to 3%	-7% to 2%	-6% to 1%	-5% to 3%	-15% to 1%	-16% to 1%
Golden, USA [114]	GNI	290-1650	2020-2021	-1% to 1%	-4% to 2%	-1% to 2%	-5% to 2%	-7% to 2%	-6% to 1%	-6% to 1%	-14% to 1%	-15% to 1%
Golden, USA [81]	DNI	350-1050	2017-2021	-2% to 2%	-11% to 0%	-2% to 3%	-15% to 0%	-19% to 1%	-18% to 0%	-20% to 1%	-18% to 1%	-22% to 1%
Hangzhou, CHN [6]	GTI	280-4000	2019-2021	-2% to 9%	-5% to 16%	-1% to 9%	-6% to 16%	-6% to 9%	-5% to 5%	-16% to 3%	-42% to 0%	-54% to 0%
Huelva, ESP [13]	DNI	350-1050	2021	-2% to 1%	-3% to -1%	-1% to 1%	-5% to -1%	-7% to -2%	-6% to -1%	-6% to 1%	-4% to 1%	-7% to 1%
Ispra, ITA [9]	GHI	400-2200	2009-2010	-3% to 4%	-4% to 7%	-3% to 4%	-4% to 8%	-5% to 4%	-4% to 3%	-10% to 3%	-35% to -2%	-47% to -2%
Jaen, ESP [19]	GTI	350-1050	2012-2019	-2% to 1%	-5% to 0%	-3% to 2%	-7% to 1%	-10% to 1%	-9% to 0%	-9% to 0%	-10% to 1%	-9% to 1%
Jaen, ESP [19]	GNI	310-1050	2011-2012	-1% to 1%	-4% to -1%	-1% to 2%	-6% to -1%	-9% to -2%	-8% to -1%	-8% to 1%	-7% to 0%	-9% to 1%
Kyoto, JPN [16]	GTI	300-1700	2018-2020	-1% to 4%	-1% to 10%	-1% to 3%	-1% to 11%	-2% to 2%	-6% to 1%	-19% to 2%	-48% to -2%	-53% to -2%
Lamont, USA [115]	GHI	350-1700	2013-2016	-3% to 1%	-11% to 2%	-3% to 1%	-13% to 3%	-15% to 2%	-14% to 1%	-15% to 0%	-13% to -3%	-15% to -2%
Lamont, USA [115]	DNI	350-1700	2013-2016	-8% to 1%	-25% to 0%	-9% to 2%	-33% to 0%	-42% to -1%	-41% to 0%	-42% to 2%	-46% to 1%	-53% to 1%
Lima, PER [24]	GTI	350-1050	2019-2020	-2% to -1%	1% to 2%	-3% to -1%	2% to 4%	-7% to -1%	-10% to -5%	-11% to -5%	-16% to -10%	-16% to -8%
Madrid, ESP [19]	GTI	350-1050	2011-2017	-3% to 1%	-9% to 8%	-3% to 1%	-13% to 11%	-16% to 1%	-15% to 0%	-28% to 0%	-16% to 0%	-15% to 0%
Manacapuru, BRA [116]	GHI	350-1700	2014-2015	-1% to 0%	-4% to 5%	-1% to 0%	-5% to 6%	-7% to 1%	-7% to 0%	-14% to 0%	-20% to -2%	-21% to -2%
Manacapuru, BRA [116]	DNI	350-1700	2014-2015	-2% to 1%	-13% to 3%	-1% to 1%	-18% to 5%	-24% to 2%	-23% to 1%	-27% to 2%	-25% to 1%	-31% to 1%
Newcastle, AUS [8]	GTI	350-1700	2017	0% to 2%	2% to 6%	0% to 2%	2% to 8%	-4% to 3%	-7% to 1%	-13% to -2%	-28% to -10%	-29% to -10%
Nicosia, CYP [9]	DNI	280-4000	2017-2018	-1% to 3%	-6% to 5%	0% to 4%	-8% to 6%	-10% to 4%	-10% to 3%	-10% to 3%	-11% to 2%	-13% to 2%
Ottawa, CAN [21]	GHI	280-4000	2018-2020	-2% to 7%	-2% to 9%	-2% to 7%	-2% to 9%	0% to 7%	-4% to 4%	-10% to 1%	-28% to -5%	-42% to -6%
Phitsanulok, THA [12]	DNI	350-1020	2007-2008	-5% to 0%	-5% to 0%	-5% to 1%	-7% to 2%	-9% to 0%	-8% to -1%	-9% to -1%	-12% to -2%	-14% to -2%
Pretoria, ZAF [15]	GTI	300-1100	2018-2021	-3% to 2%	-1% to 2%	-3% to 2%	-2% to 3%	-5% to 2%	-8% to 2%	-9% to 2%	-15% to -2%	-14% to -4%
Roskilde, DEN [2]	GHI	300-1050	2020-2021	-2% to 1%	0% to 1%	-3% to 1%	-1% to 2%	-4% to 1%	-7% to 1%	-9% to 1%	-13% to -4%	-11% to -6%
Roskilde, DEN [2]	DNI	300-1050	2020-2021	0% to 3%	-5% to 0%	1% to 4%	-10% to 0%	-16% to -1%	-15% to 0%	-18% to 2%	-17% to 1%	-25% to 2%
São José dos Campos, BRA [18]	GHI	350-1050	2013-2015	-1% to 3%	-2% to 6%	-1% to 2%	-2% to 7%	-3% to 2%	-5% to 0%	-11% to 0%	-3% to -2%	-4% to -2%
São Paulo, BRA [28]	GHI	350-1050	2019	-3% to 0%	2% to 3%	-3% to 1%	3% to 5%	-7% to 2%	-11% to -2%	-12% to -2%	-18% to -8%	-19% to -9%
Singapore, SGP [22]	GTI	350-1050	2019-2021	-4% to -2%	1% to 9%	-4% to -2%	2% to 14%	-22% to -1%	-25% to -5%	-32% to -5%	-38% to -11%	-42% to -11%
Utrecht, NLD [23]	GTI	350-1050	2014-2017	-2% to 1%	-6% to 1%	-2% to 1%	-10% to 2%	-13% to 1%	-12% to 0%	-15% to 2%	-13% to 1%	-16% to 1%
Vienna, AUT [17]	GHI	350-1600	2019-2021	0% to 2%	-2% to 5%	0% to 2%	-3% to 6%	-4% to 3%	-3% to 2%	-10% to 1%	-31% to -2%	-34% to -2%

Acknowledgements

The authors are grateful for the spectral irradiance data provided online: by the U.S. Department of Energy via the Atmospheric Radiation Measurement (ARM) user facility, the National Renewable Energy Laboratory (NREL), and Sandia National Laboratories; the University of Oregon; and the National Institute of Standards and Technology (NIST).

SERIS is a research institute at the National University of Singapore (NUS). SERIS is supported by NUS, the National Research Foundation Singapore (NRF), the Energy Market Authority of Singapore (EMA) and the Singapore Economic Development Board (EDB).

Data from Ispra, Italy (Matthew Norton, Ana Gracia Amillo, Roberto Galleano) was supported by the Joint Research Centre of the European Commission.

Data from Huelva, Spain (Gabriel López) was supported by the Spanish Ministry of Economy, Industry, and Competitiveness “PVCastSOIL” project No ENE2017-83790-C3-1-2-3-R, in collaboration with the European Regional Development Fund.

M. Braga and R. Rüter acknowledge financial support of the Brazilian Electricity Regulatory Agency – ANEEL through the ANEEL R&D Program.

J. A. Töfflinger and M. A. Sevillano-Bendezú acknowledge the financial support by the Peruvian CONCYTEC PROCIENCIA through Contract 013-2020-FONDECYT-BM.

Data from Kusatu, Japan (Takashi Minemoto) was supported by the New Energy and Industrial Technology Development Organization (NEDO), Japan.

Appendix & Supplemental Information

A. Standard spectra

There are three standard solar spectra for space and terrestrial solar applications: AM0, AM1.5D, and AM1.5G. “AM,” short for “air mass,” is the hypothetical column of air between the sun and the incident surface. AM0 (defined in 1974), is used for solar cells under extraterrestrial radiation (zero air mass). An air mass of one (“AM1”) is the condition when the sun is directly overhead. The standard terrestrial spectrum was established by the American Society for Testing and Materials (ASTM) in 1982, at a time when AM1.5 was considered representative of a “typical” solar module: one tilted at a fixed angle of 37° (mid-latitude USA) and pointed due south.

AM1.5D is the ASTM “direct” spectrum for this orientation, intended to represent only the sunlight coming directly from the sun (or its near vicinity). AM1.5D finds practical application in systems using two-axis trackers and optical concentration (lenses or mirrors) to boost solar cells’ power and efficiency. These optical concentrators are effective in concentrating only the collimated rays that come directly from the solar disc. The “global” spectrum, AM1.5G, consists of these direct rays, as well as sunlight that has been scattered by the atmosphere and is arriving on the tilted surface from the hemispherical dome of the sky. The “AM1.5” spectrum in international standard IEC 61853 is defined in IEC 60904-03 and is consistent with AM1.5G, as defined by ASTM G173-03.

B. Efficiency, power, and energy: predicted, expected, and measured

Efficiency has been used as the figure of merit due to its general familiarity and area independence. The largest increases in relative efficiency are seen in cells with the narrowest spectral response (cadmium telluride and single-junction perovskite). Since efficiency is the ratio of power output to power input, it should be noted that efficiency rise due to spectrum variation may be due either to an increase in the power provided by the cell, or a decrease in the irradiance outside the cell’s spectral response range: higher efficiency does not always imply higher power. This is illustrated in Figure 7, where two spectra are presented that deliver the same output power in a cadmium telluride cell, but different efficiencies. While the broadband irradiance in the arid climate of Albuquerque is 7% higher, the excess falls outside the spectral response range of cadmium telluride. As a result, the two current densities integrate to the same value: 302 A/m², giving a cell output power density of 210 W/m² for both. The efficiency, however, is 21.5% for Albuquerque and 23.0% for Sao José dos Campos.

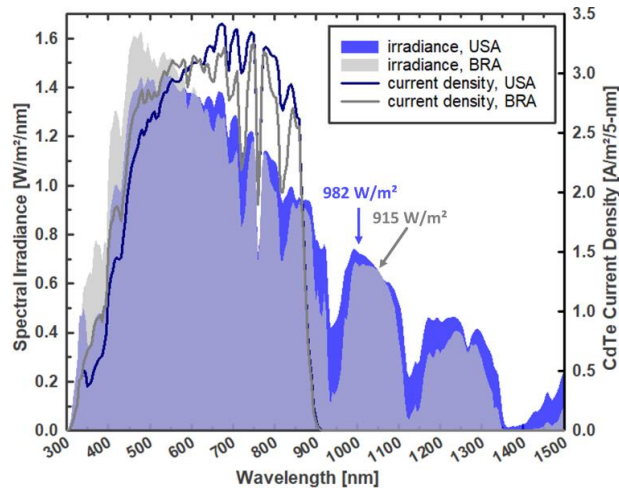


Figure 7. Spectral irradiance and the resulting current density for cadmium telluride from cherry-picked weekly sums found in the Albuquerque (USA) and Sao José dos Campos (BRA) data sets. Cadmium telluride has a spectral response range of ~300-900 nm. The two resulting current density lines form equal areas.

For the purposes of comparing different PV technologies, assessing power plant operation, and evaluating warranty claims, the power rating (in watts) is defined under a set of standard conditions. In windless conditions, the temperature, broadband irradiance, and spectral radiance define the standard. The international standard for module power rating, IEC 61853-1, provides four temperatures, four broadband irradiances, and one spectrum. IEC 61853 also defines an energy rating using six climatic profiles, assuming a fixed tilt angle of 20°. For each zone, standard temperature, broadband irradiance, and irradiance divided into twenty-eight wavelength bands have been tabulated at hourly intervals for a representative year. For comparison with the measured data, the bands have been converted to spectral irradiance at 5-nm intervals; the resulting cell efficiencies are included in Appendices F, O, and L.

The power and energy ratings are *predicted* results, in that they rely on models and historical meteorological data. Between the *predicted* and *measured* results, there are also *expected* results, which employ contemporaneous measured meteorological data as inputs to the models¹¹⁷. The denominator in the performance ratio discussed above is one example, as it takes the power rating and corrects for the measured broadband irradiance (and often, temperature). As an alternative to direct measurement, the expected spectral irradiance can be determined by measuring site pressure and the atmospheric compositions of aerosols, precipitable water, ozone, and CO₂⁸¹. Instruments to measure the atmospheric composition (sun photometers) similarly employ radiometry, at specific wavelengths, so using this method to determine the spectrum is a somewhat circular process.

C. Measurement accuracy and uncertainty

The uncertainty in spectroradiometer measurements varies as a function of wavelength range and sensor design; representative values can be found in [118] and [119]. Since 2011, measurement accuracy among manufacturers has been verified annually in the International Spectroradiometer Intercomparison¹²⁰. In field operation, the sensors require periodic re-calibration¹²¹ and maintenance to remove soiling and verify temperature stability. The calibration and maintenance histories of the sensors used in this study are maintained by the respective authors.

D. Substitution of AM1.5 for values outside the measurement range

The AM1.5 standard spectrum is defined for a wavelength range of 280-4000 nm²⁵. Spectroradiometers measure only some portion of this range (Table 1). For values outside the measurement range, AM1.5 values were substituted. Other approaches are possible (using scaled values, e.g.), but use of fixed AM1.5 values results in performance variation that is more of a lower bound. Normalization of the weekly spectral irradiance magnitudes was made at either 880 nm or 1050 nm, wavelengths at which atmospheric variation is at a minimum: the difference between AM1.5 and the solar constant in space (AM0) is less than 1% at these wavelengths^{24,25}. 1050 nm was used for most locations, but 880 nm was used in cases (Singapore, e.g.) where the atmospheric absorption in the near infrared is substantially higher than for AM1.5, so normalization at 1050

nm could result in anomalous values that exceed AM0. For the four- and six-junction III-Vs, any data for which one or more junctions fall outside the measurement range is excluded from the results.

The sensitivity of the cell performance variation to this method was evaluated using data from sensors that measure data beyond 1050 nm. Data from 1050-4000 nm was substituted with AM1.5 values; comparisons are shown in Figure 8.

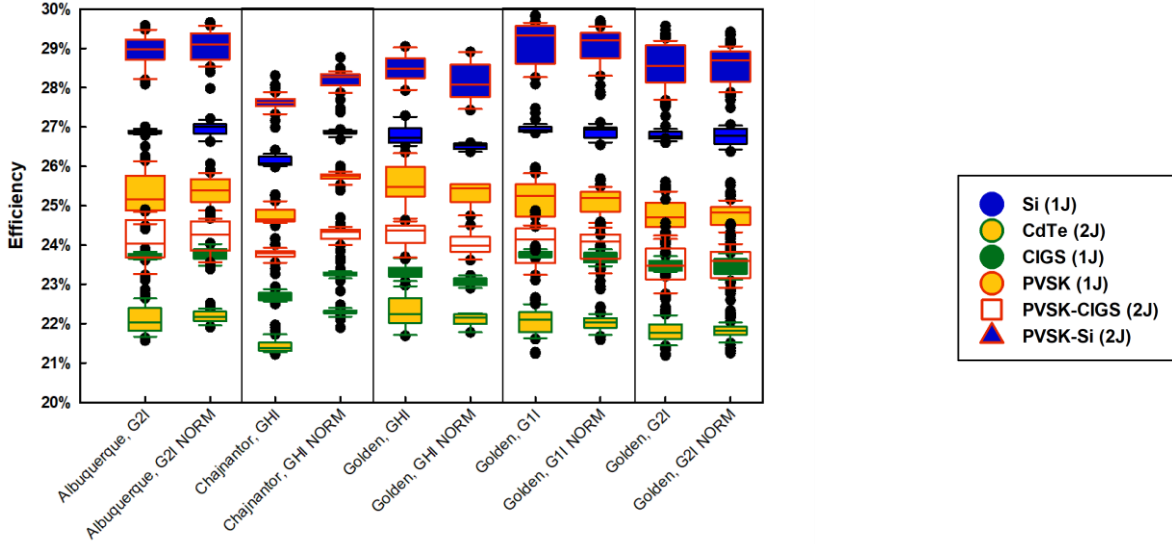


Figure 8. Sensitivity of performance variation to the normalization method in Appendix D. For each site, the left-hand data contains the full measurement range (Table 1); for the right-hand data (labeled “NORM”), measured values beyond 1050 nm have been substituted with AM1.5 values.

E. Calculation of cell efficiency from the quantum efficiency

Cell efficiencies are calculated using the open-circuit voltage (V_{oc}) and fill factor (FF) confirmed under Standard Test Conditions (25°C , 1000 W/m^2 , AM1.5 spectrum). Variations in spectral irradiance are assumed to affect only the cell short-circuit current. Second-order effects, such as changes to voltage or fill factor with changing irradiance¹²², or increases in fill factor in multijunctions due to current mismatch⁴⁶ are not considered here. The short-circuit current is derived from a cell’s spectral response and quantified using the cell quantum efficiency, which is a measure of the percentage of incoming photons at each wavelength that are absorbed and converted into current. Quantum efficiencies obtained from the Solar Cell Efficiency Tables are digitized at 5-nm wavelength intervals. Since the amplitude of the published quantum efficiencies is often normalized, the amplitudes are scaled to obtain the short-circuit current confirmed under the standard spectrum, AM1.5G (AM1.5D, for the III-V multijunctions)²⁸.

To obtain the current generated under a given spectrum, the spectral irradiance (G_λ) is divided by the photon energy at each wavelength (E_λ) to give the number of photons in that interval (5-nm intervals are used in this study). Multiplying by the quantum efficiency (QE_λ) gives the “spectral current density” [$\text{A/m}^2/\text{nm}$] that would be converted to current at that wavelength. Multiplying by the wavelength interval ($\Delta\lambda$) yields current density [mA/cm^2] for each interval; summing over all wavelengths obtains the short-circuit current density (J_{sc}):

$$J_{sc} = \sum_{\lambda} \left(\frac{G_{\lambda}}{E_{\lambda}} \right) \cdot QE_{\lambda} \cdot \Delta\lambda$$

The product $V_{oc} \cdot \text{FF} \cdot J_{sc}$ is then the cell power density [W/m^2]. Dividing by the broadband irradiance [W/m^2] obtains the cell efficiency.

Once the quantum efficiency of a given cell type is known, the current density (and cell efficiency) under a standard spectrum can be used to determine the current density under a second spectrum by applying a spectrum mismatch correction⁹⁵.

F. Absolute efficiency

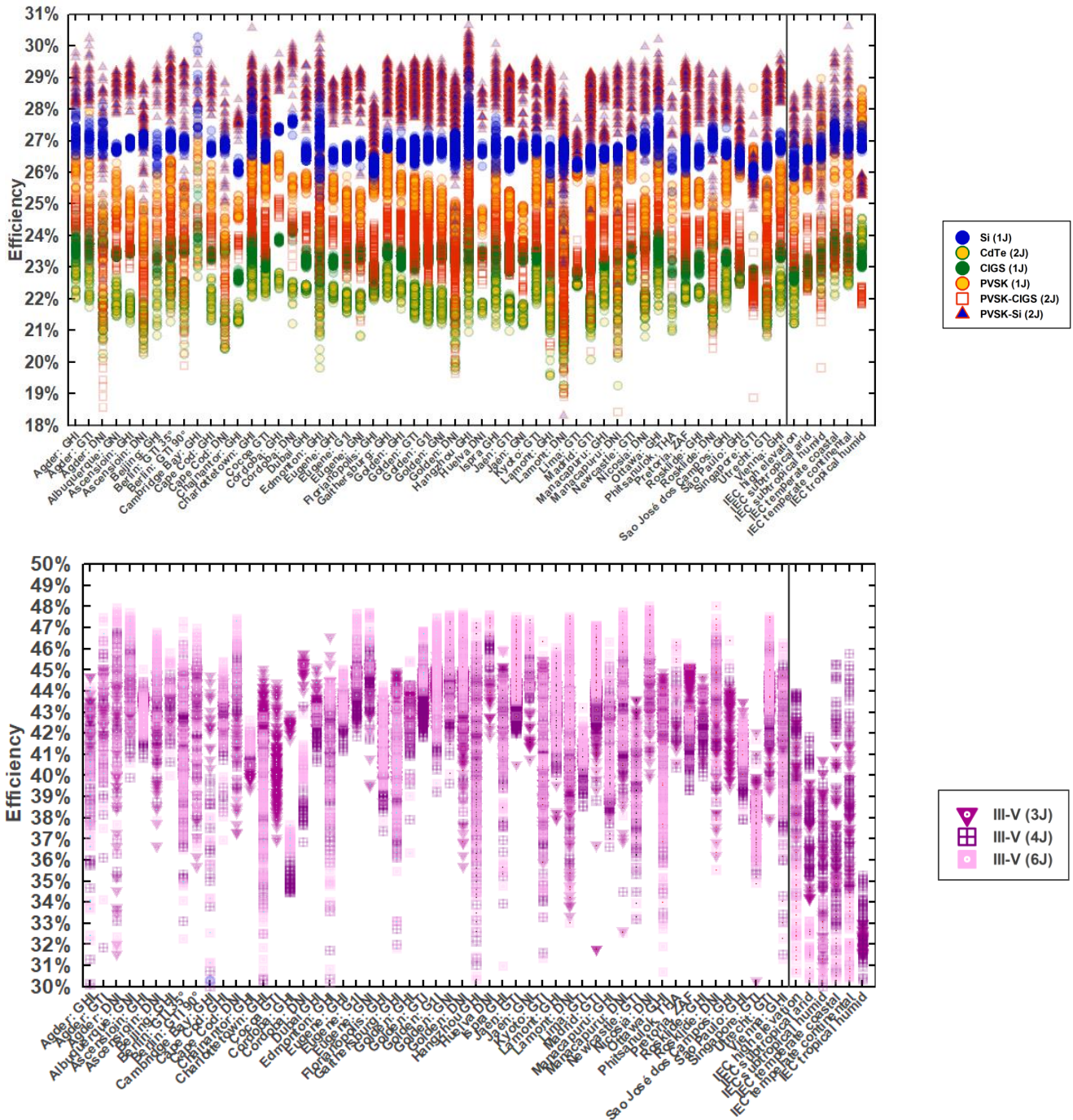


Figure 9. Efficiency as a function of location and orientation. Results adapted from the spectral bands for the six IEC 61853 reference climatic profiles are included on the right.

G. Measured vs. synthetic spectra

Models for solar spectral irradiance enable synthesis of spectral using input atmospheric conditions⁷⁴, such as site pressure and the aerosol, water vapor, ozone, and CO₂ levels. Inputs are sourced from both satellite radiometer telemetry (NOAA/NASA GOES-R) and ground-based atmosphere radiometers. The National Solar Radiation Database at NREL hosts Spectral On-Demand, a tool accessible online as part of the satellite-derived data in the NSRDB Data Viewer¹²³. Spectral On-Demand synthesizes spectra from past years within an area defined by NREL's Physical Solar Model¹²⁴. The synthetic spectra below tend to show more irradiance in the visible wavelength range (400-700 nm) than is found in the measured spectra. The extent to which a given synthetic or measured spectrum best represents the "ground truth" at a location requires further analysis of both. Measured spectral data was obtained from a variety of sensors, from different manufacturers, so the offset between measured and synthetic spectra is suggestive of a systematic difference between site spectroradiometers and the models and radiometer telemetry used to produce the synthetic results. As

demonstrated in [39], output of PV modules with different spectral responses could be used to resolve the discrepancies.

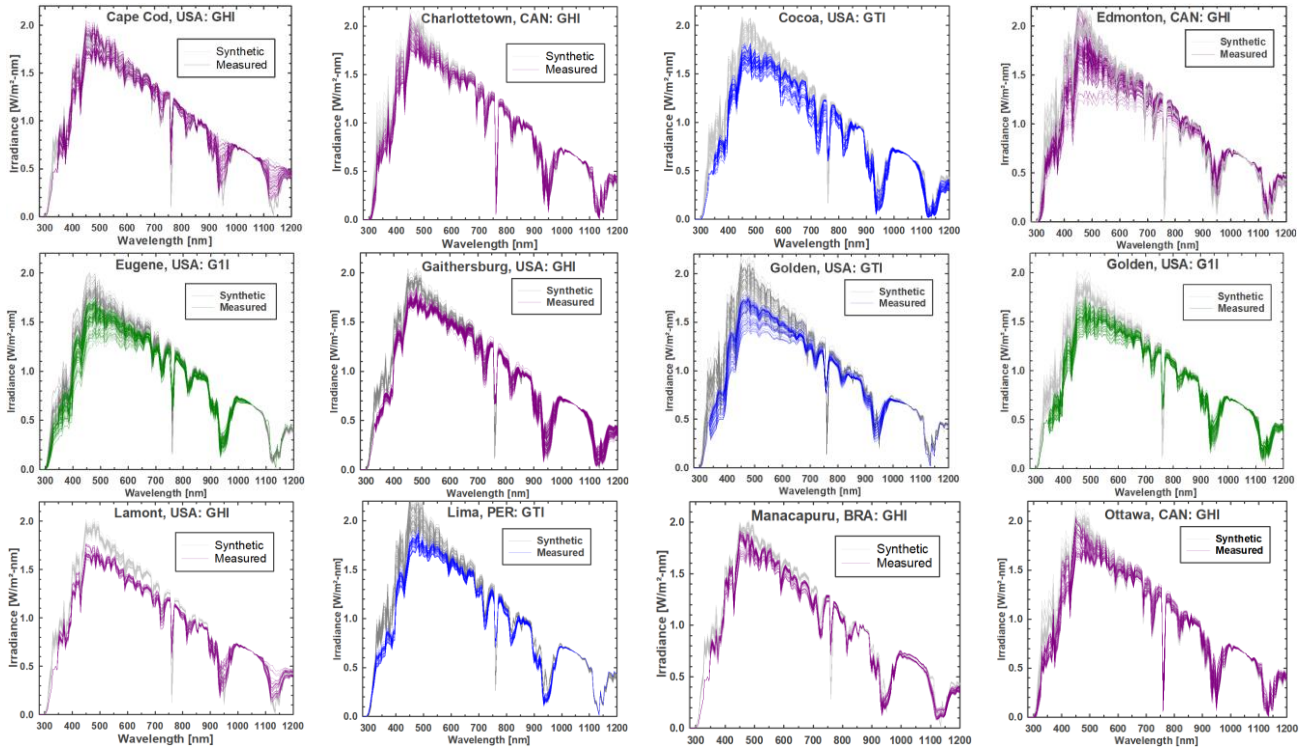


Figure 10. Measured weekly spectra (colors) compared against synthetic (gray) spectra from NREL's Spectral On-Demand.

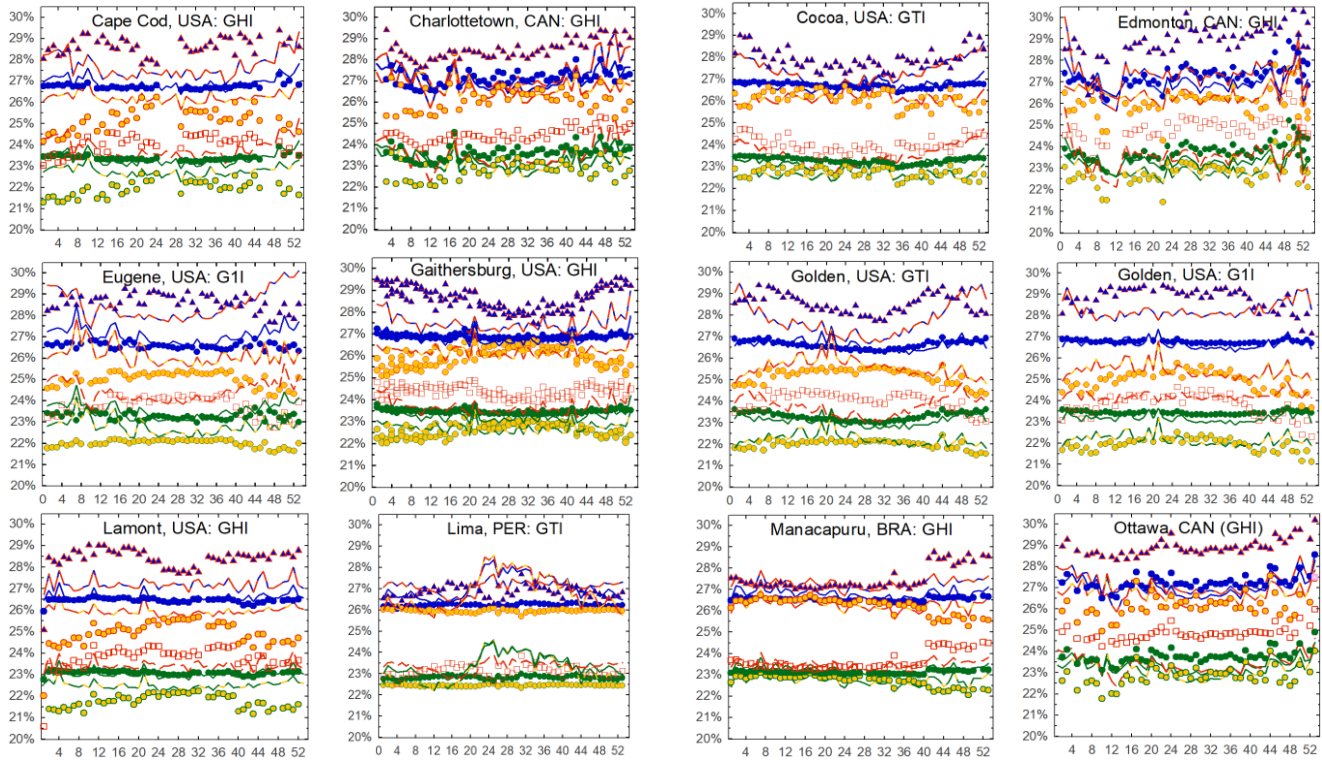


Figure 11. Measured (symbols) vs. synthetic spectra (lines) for sites currently available from NREL's Physical Solar Model¹²³ (longitude: -25°E to -175°W, latitude: -20°S to 60°N).

H. Efficiency vs. orientation

As seen in analyses of synthetic spectra^{28,48,49}, increases in the amount of sun tracking increase the degree of spectral variation and therefore tend to be less favorable for cells with a narrower spectral response. As the degree of tracking increases in Figure 12 below, efficiency tends to increase for single-junction cells with a wider spectral response (Si, CIGS) and decreases for the cells with a narrower response (CdTe, PVSK).

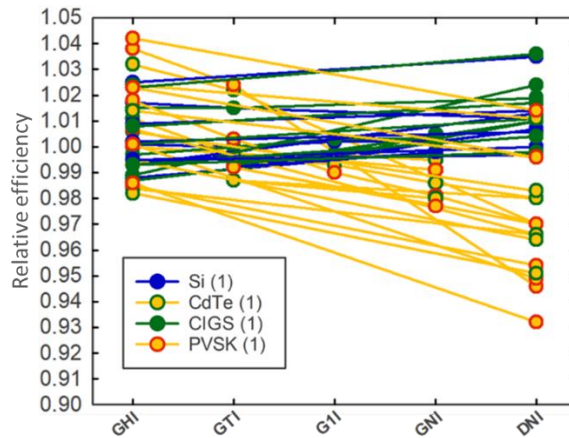


Figure 12. Comparison of relative median efficiency of single-junction cells for sites with more than one sensor orientation: Agder, NOR; Ascension Island, BOT; Cape Cod, USA; Córdoba, ARG; Eugene, USA; Golden, USA; Lamont, USA; Manacapuru, BRA, Jaén, ESP; Roskilde, DEN.

I. Median efficiency vs. site latitude

While Figure 5 is suggestive of a relation between site latitude and efficiency, other driving (atmospheric) factors such as site pressure, water vapor, and aerosols are often co-variant with latitude. Latitude, alone, is not a strong predictor of the impact of spectral irradiance variation.

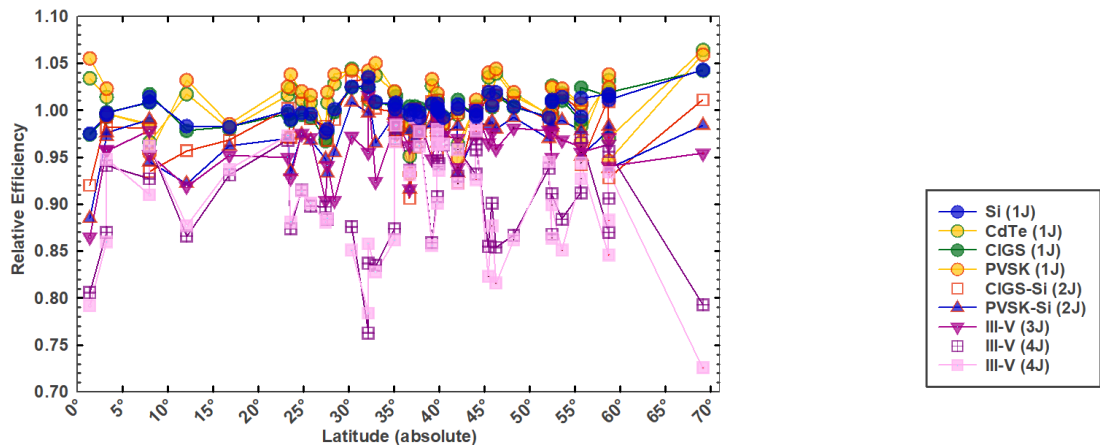


Figure 13. Site median of weekly relative efficiency as a function of the absolute value of site latitude.

J. Worldwide variation in silicon efficiency under global irradiances (GHI, GTI, G1I, GNI)

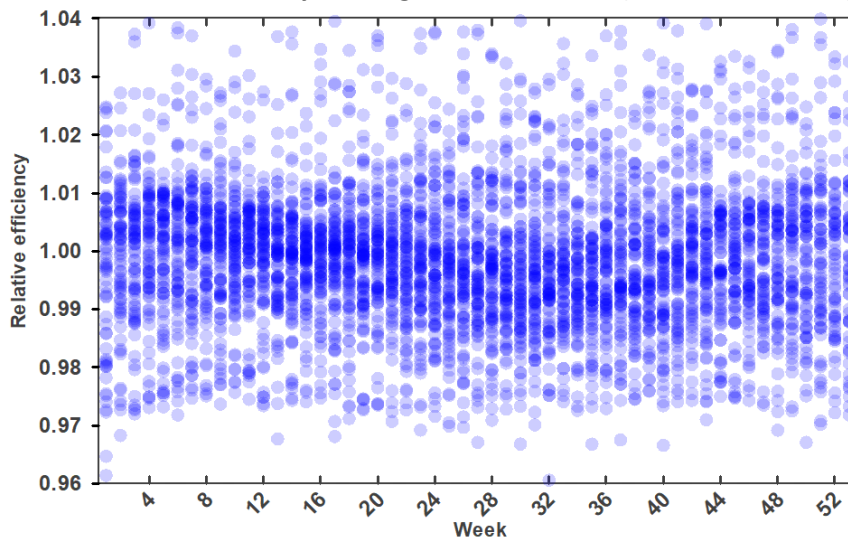
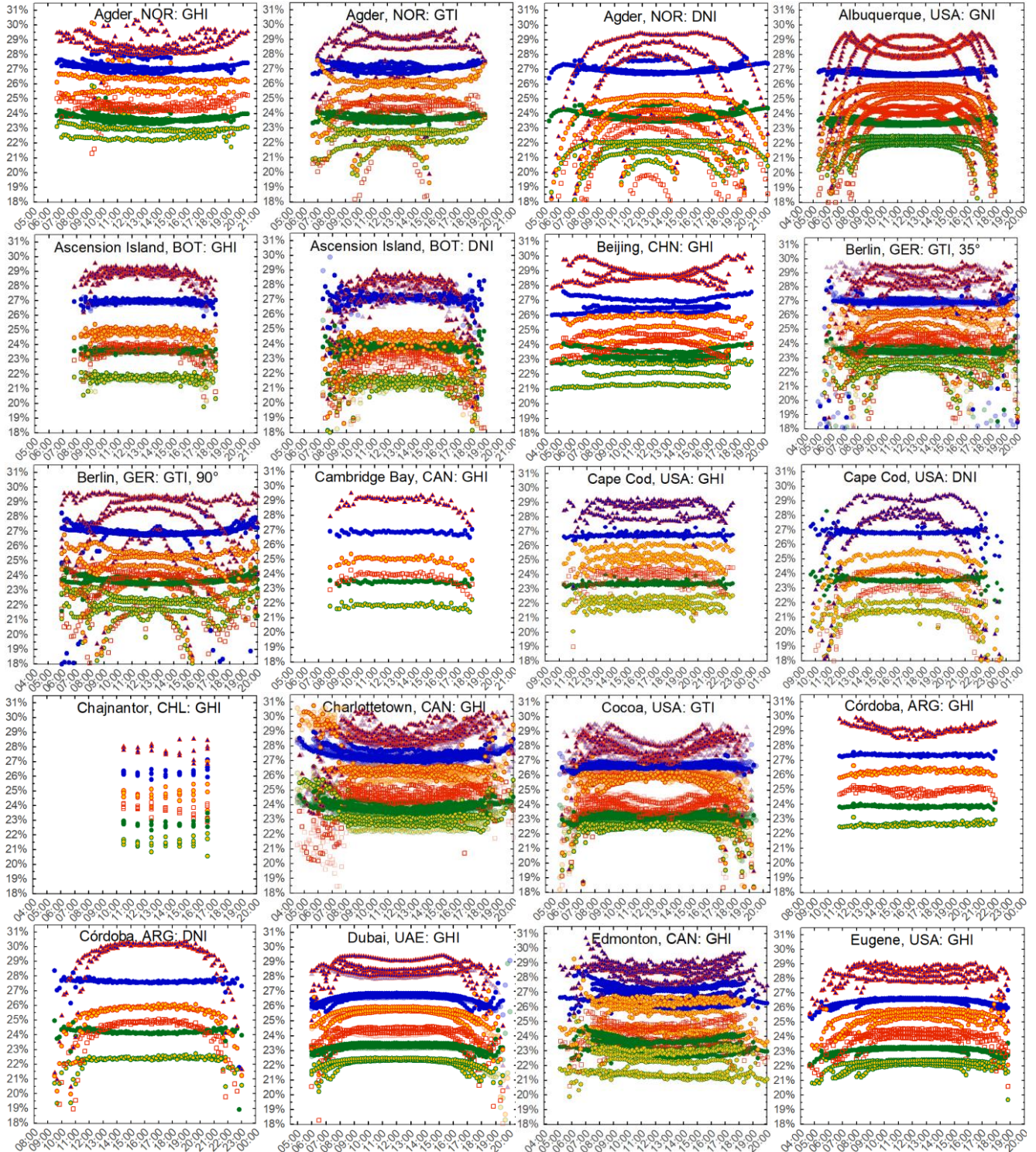
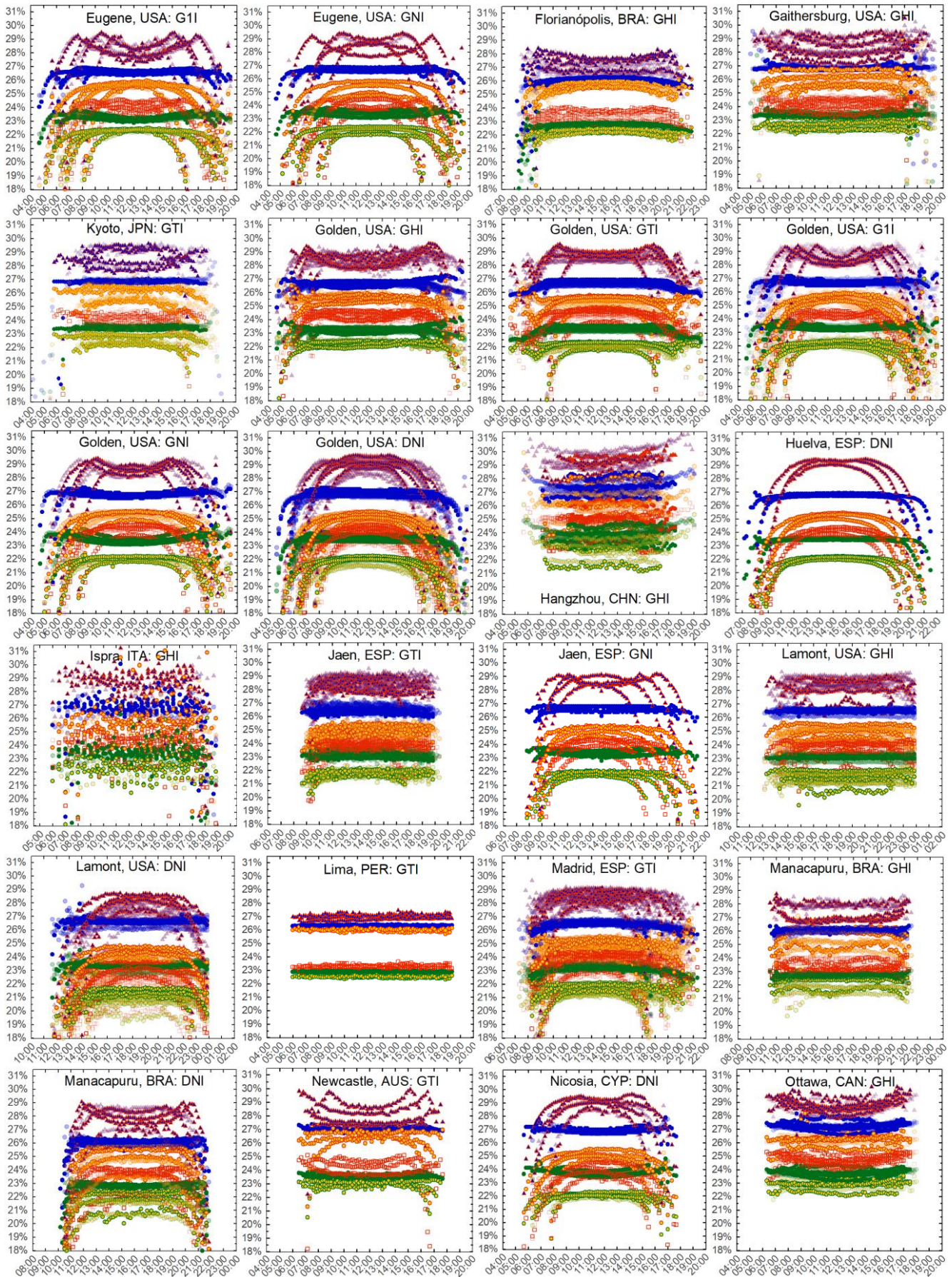


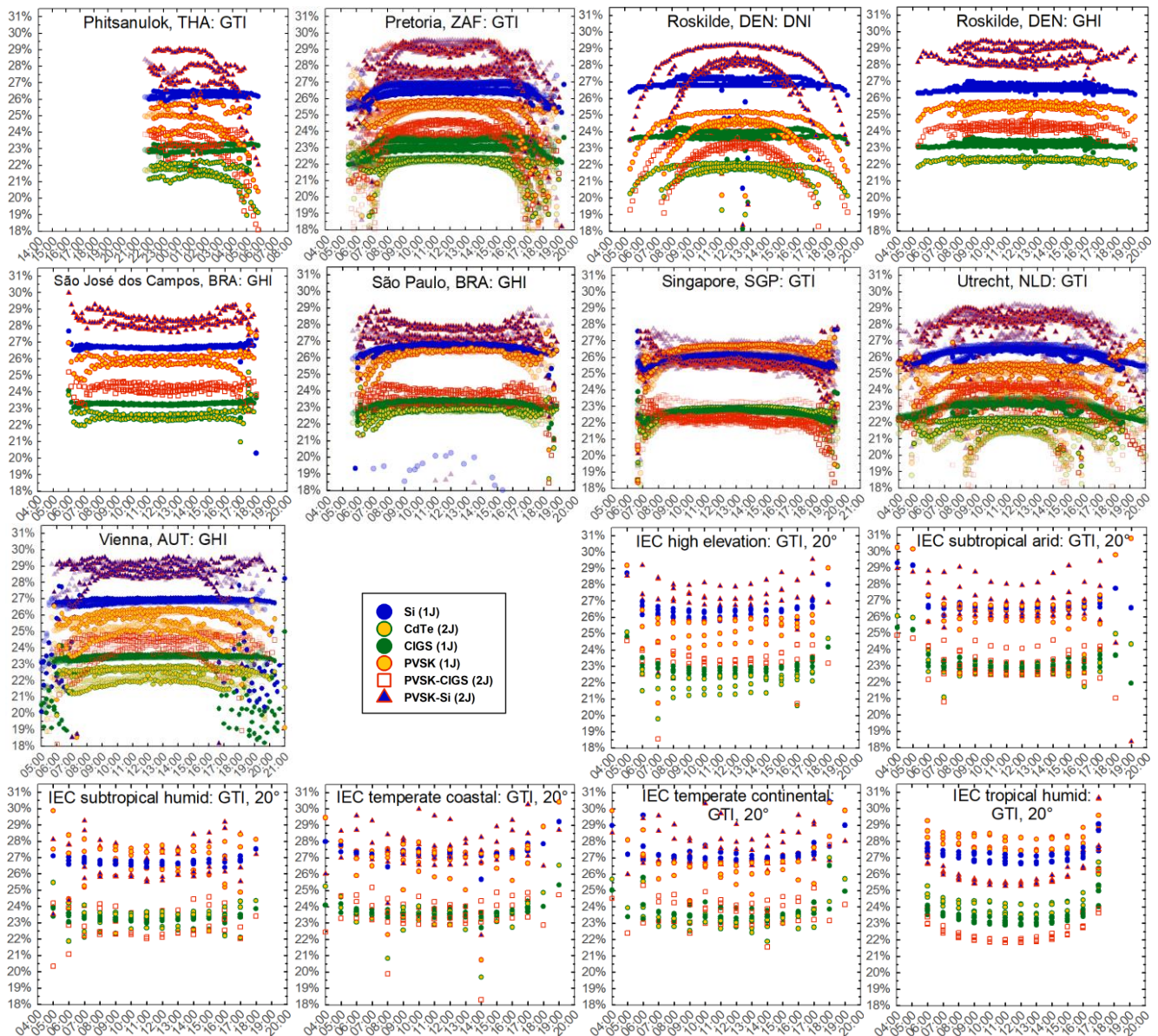
Figure 14. Relative weekly efficiency of silicon under spectral variations in global irradiance (GHI, GTI, G1I, GNI).

K. Diurnal and seasonal variation

Seasonal and diurnal efficiency variations for cells with one or two junctions. Seasonal changes are delineated using one month of data for March, June, September, and December. Where available, data from other years is semi-transparent in the background. Data is sampled at 10-minute intervals for each month, except at Chajnantor (60-minute interval). Time basis may be either local or GMT. For comparison, values derived from the six climatic zones in IEC 61853-4 are included at the bottom.

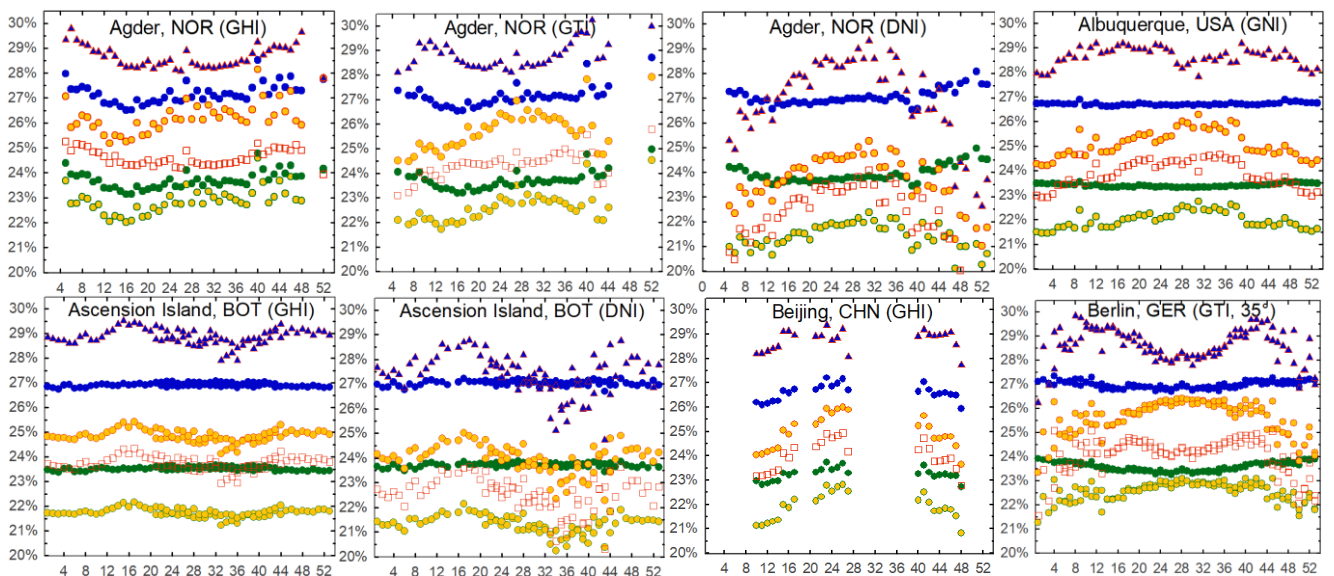


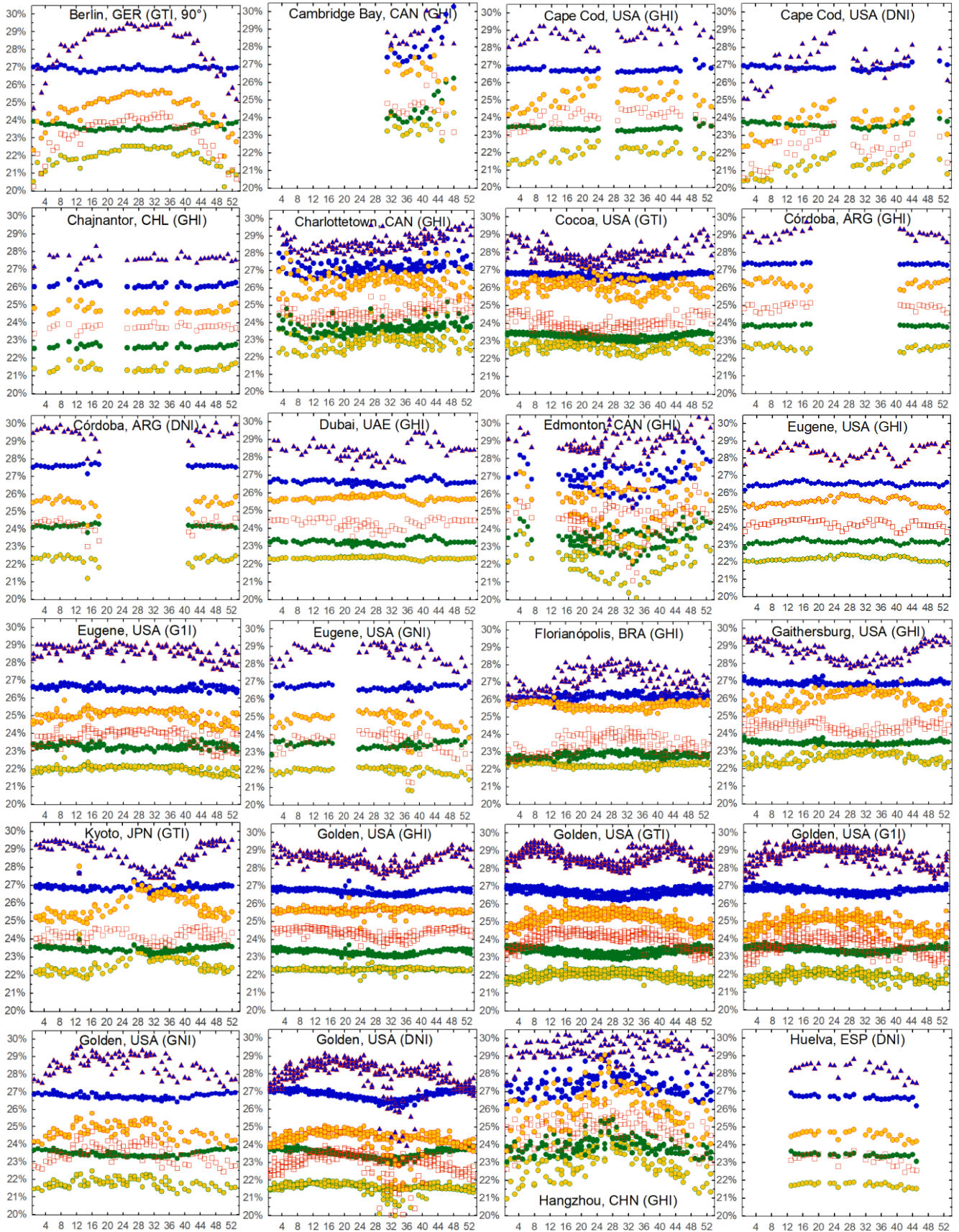


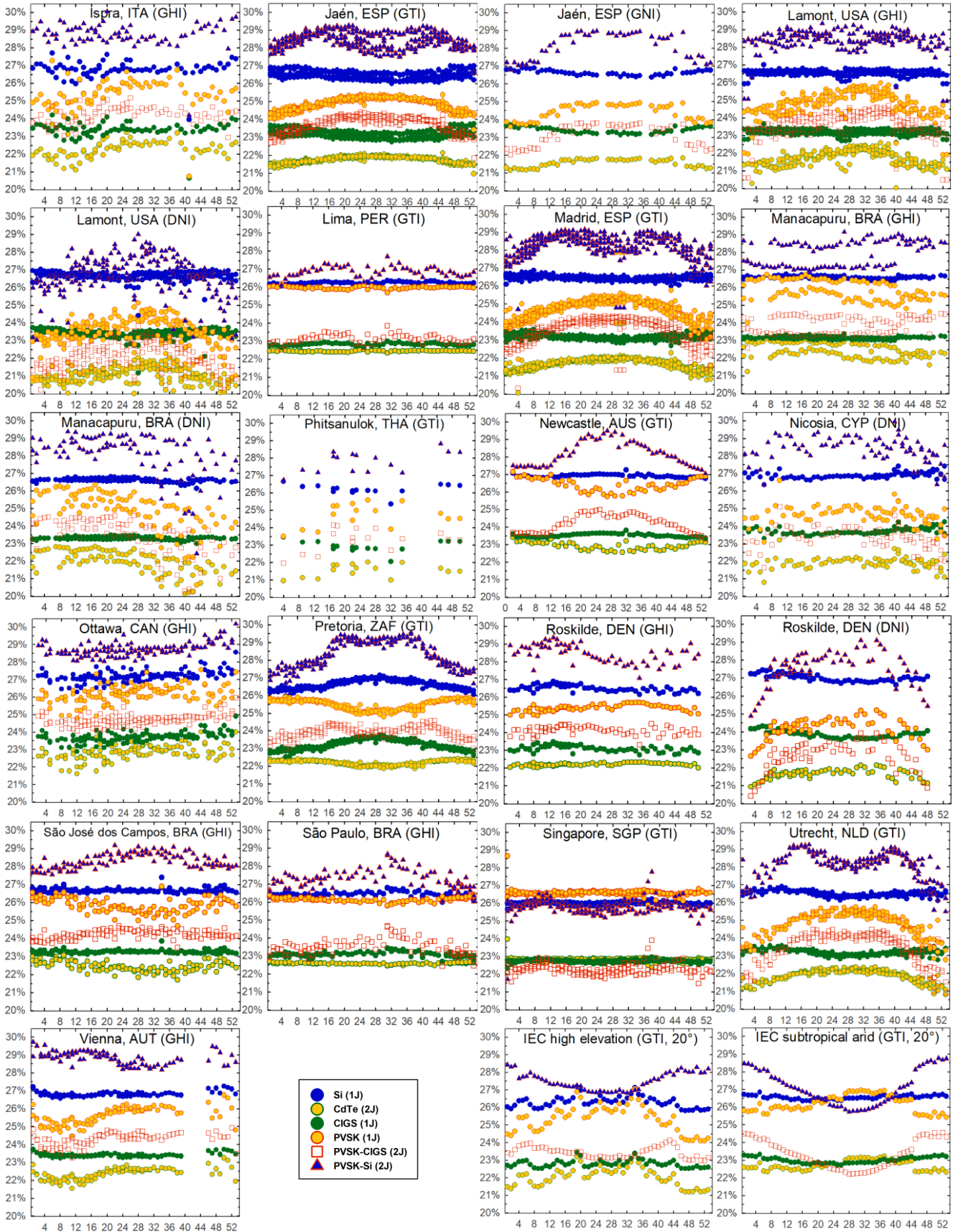


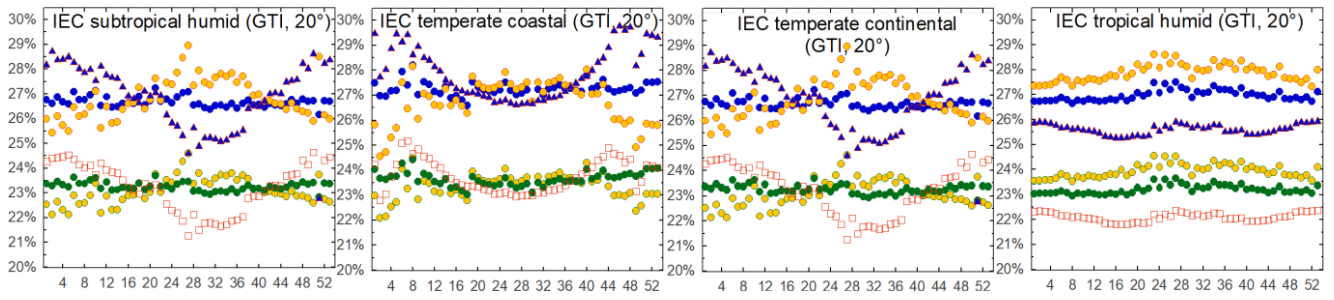
L. Annual efficiency variation: absolute efficiency vs. week of the year for one- and two-junction cells

As above, each week is a summation of data sampled at 10-minute intervals except at Chajnantor (60-minute interval). For comparison, values derived from the six climatic zones in IEC 61853-4 are included at the bottom.









References

1. Faine, P., Kurtz, S. R., Riordan, C. & Olson, J. M. The influence of spectral solar irradiance variations on the performance of selected single-junction and multijunction solar cells. *Solar Cells* **31**, 259–278 (1991).
2. Krauter, S. & Hanitsch, R. Actual optical and thermal performance of PV-modules. *Solar Energy Materials and Solar Cells* **41–42**, 557–574 (1996).
3. Nann, S. & Emery, K. Spectral effects on PV-device rating. *Solar Energy Materials and Solar Cells* (1992) doi:10.1016/0927-0248(92)90083-2.
4. Schweiger, M. Impact of spectral irradiance on energy yield of PV modules measured in different climates. *4th PV Performance Modelling and Monitoring 17 Workshop* (2015) doi:10.13140/RG.2.2.33591.73122.
5. Kinsey, G. S. Spectrum sensitivity, energy yield, and revenue prediction of PV modules. *IEEE Journal of Photovoltaics* **5**, (2015).
6. Nofuentes, G., García-Domingo, B., Muñoz, J. v. & Chenlo, F. Analysis of the dependence of the spectral factor of some PV technologies on the solar spectrum distribution. *Applied Energy* **113**, 302–309 (2014).
7. Minemoto, T., Nagae, S. & Takakura, H. Impact of spectral irradiance distribution and temperature on the outdoor performance of amorphous Si photovoltaic modules. *Solar Energy Materials and Solar Cells* (2007) doi:10.1016/j.solmat.2007.02.012.
8. Myers, D. R., Emery, K. & Gueymard, C. Revising and validating spectral irradiance reference standards for photovoltaic performance evaluation. in *International Solar Energy Conference* (2002). doi:10.1115/SED2002-1074.
9. Hirata, Y. & Tani, T. Output variation of photovoltaic modules with environmental factors—I. The effect of spectral solar radiation on photovoltaic module output. *Solar Energy* **55**, 463–468 (1995).
10. Lindsay, N., Libois, Q., Badosa, J., Migan-Dubois, A. & Bourdin, V. Errors in PV power modelling due to the lack of spectral and angular details of solar irradiance inputs. *Solar Energy* **197**, 266–278 (2020).
11. Solar projects are underperforming by 6.3%: New report suggests better assessment standards. <https://www.solarpowerworldonline.com/2020/10/solar-projects-are-underperforming-by-6-3-new-report-suggests-better-assessment-standards/>.
12. Wang, Y., Millstein, D., Mills, A. D., Jeong, S. & Ancell, A. The cost of day-ahead solar forecasting errors in the United States. *Solar Energy* **231**, 846–856 (2022).
13. The lurking threat to solar power's growth | MIT Technology Review. <https://www.technologyreview.com/2021/07/14/1028461/solar-value-deflation-california-climate-change/>.
14. IEC. IEC 60904-1 Ed. 2.0 b:2006 - Photovoltaic devices - Part 1: Measurement of photovoltaic current-voltage characteristics. IEC https://webstore.ansi.org/Standards/IEC/IEC60904Ed2006?gclid=Cj0KCQjw7MGJBhD-ARIsAMZ0eeuLqyJsaU8ouzY8cQhNxdJTJaTplxixyA_XhrmcN8dzjFILhwwzBW0aAsRIEALw_wcB (2006).
15. Reich, N. H. *et al.* Performance ratio revisited: is PR > 90% realistic? *Progress in Photovoltaics: Research and Applications* **20**, 717–726 (2012).
16. NREL. Reference Air Mass 1.5 Spectra | Grid Modernization | NREL. <https://www.nrel.gov/grid/solar-resource/spectra-am1.5.html>.

17. Wilson, H. R. Effect of solar spectral variation on solar cell short circuit current: results of long-term continuous measurements. *Seventh E.C. Photovoltaic Solar Energy Conference* 309–313 (1987) doi:10.1007/978-94-009-3817-5_57.
18. Riordan, C. & Hulstrom, R. Outdoor spectral solar radiation variations and their relationship to photovoltaic device performance. *Current topics in photovoltaics* 1–23 https://inis.iaea.org/search/search.aspx?orig_q=RN:23072299 (1990).
19. IEC. IEC 60891 Ed. 2.0 b:2009 - Photovoltaic devices - Procedures for temperature and irradiance corrections to measured I-V characteristics. <https://webstore.ansi.org/Standards/IEC/IEC60891Ed2009> (2009).
20. Trina Solar. Utility Scale Solar Panels - Trina Solar. <https://www.trinasolar.com/us/product/utility> (2021).
21. Jinko Solar. *LIMITED WARRANTY*. www.jinkosolar.com (2020).
22. IEC. IEC 61724 Ed. 1.0 b:1998 - Photovoltaic system performance monitoring - Guidelines for measurement, data exchange and analysis. https://webstore.ansi.org/Standards/IEC/IEC61724Ed1998?gclid=Cj0KCQjwpreJBhDvARIsAF1_BU1KSICweyVqr2NGsnJJEWBJBzH1TJVw28jHUdoGUdo2Bgb9_RMeodQaAgkpEALw_wcB (1998).
23. IEC. IEC 61853-1 Ed. 1.0 b:2011 - Photovoltaic (PV) module performance testing and energy rating - Part 1: Irradiance and temperature performance measurements and power rating. https://webstore.ansi.org/Standards/IEC/IEC61853Ed2011?gclid=CjwKCAjwybyJBhBwEiwAvz4G7zGGe1v53mSa7VebpR9Olf3ZvBe-uj7mNzKvhAxoSPOoTrqdBclnCRoCoqlQAvD_BwE (2011).
24. ASTM. *ASTM E490-00a (2019), Solar Constant and Zero Air Mass Solar Spectral Irradiance Tables*. ASTM International (2004).
25. ASTM G173-03. *G173-03(2012) Standard Tables for Reference Solar Spectral Irradiances: Direct Normal and Hemispherical on 37° Tilted Surface*. ASTM International (2012).
26. Solar - Fuels & Technologies - IEA. <https://www.iea.org/fuels-and-technologies/solar>.
27. Pricing Carbon. <https://www.worldbank.org/en/programs/pricing-carbon>.
28. Kinsey, G. S. Solar cell efficiency divergence due to operating spectrum variation. *Solar Energy* **217**, 49–57 (2021).
29. Snapshot 2021 - IEA-PVPS. <https://iea-pvps.org/snapshot-reports/snapshot-2021/>.
30. Renewable Energy Agency, I. *Global Energy Transformation: A Roadmap to 2050*. (2018).
31. Europe – Countries & Regions - IEA. <https://www.iea.org/regions/europe>.
32. Castro, J. B. et al. *International Technology Roadmap for Photovoltaic (ITRPV), 9th Edition*. <https://itrpv.org/> (2018).
33. *International Technology Roadmap for Photovoltaic (ITRPV), 12th edition*. (2020).
34. NREL. Best Research-Cell Efficiency Chart | Photovoltaic Research | NREL. <https://www.nrel.gov/pv/cell-efficiency.html> (2020).
35. Fernandez, E. F., Cruz, F. A., Mallick, T. K. & Sundaram, S. Effect of Spectral Irradiance Variations on the Performance of Highly Efficient Environment-Friendly Solar Cells. *IEEE Journal of Photovoltaics* (2015) doi:10.1109/JPHOTOV.2015.2434593.

36. Alonso-Abella, M., Chenlo, F., Nofuentes, G. & Torres-Ramírez, M. Analysis of spectral effects on the energy yield of different PV (photovoltaic) technologies: The case of four specific sites. *Energy* (2014) doi:10.1016/j.energy.2014.01.024.
37. Huld, T. & Gracia Amillo, A. M. Estimating PV module performance over large geographical regions: The role of irradiance, air temperature, wind speed and solar spectrum. *Energies* (2015) doi:10.3390/en8065159.
38. Norton, M., Amillo, A. M. G. & Galleano, R. Comparison of solar spectral irradiance measurements using the average photon energy parameter. *Solar Energy* **120**, 337–344 (2015).
39. Dirnberger, D., Blackburn, G., Müller, B. & Reise, C. On the impact of solar spectral irradiance on the yield of different PV technologies. *Solar Energy Materials and Solar Cells* **132**, 431–442 (2015).
40. Cornaro, C. & Andreotti, A. Influence of Average Photon Energy index on solar irradiance characteristics and outdoor performance of photovoltaic modules. *Progress in Photovoltaics: Research and Applications* (2013) doi:10.1002/pip.2194.
41. Ishii, T., Otani, K., Takashima, T. & Xue, Y. Solar spectral influence on the performance of photovoltaic (PV) modules under fine weather and cloudy weather conditions. *Progress in Photovoltaics: Research and Applications* (2013) doi:10.1002/pip.1210.
42. Kinsey, G. S. Spectrum sensitivity, energy yield, and revenue prediction of PV and CPV modules. in *2015 IEEE 42nd Photovoltaic Specialist Conference, PVSC 2015* (2015). doi:10.1109/PVSC.2015.7355850.
43. Lee, M., Ngan, L., Hayes, W. & Panchula, A. F. Comparison of the effects of spectrum on cadmium telluride and monocrystalline silicon photovoltaic module performance. in *2015 IEEE 42nd Photovoltaic Specialist Conference, PVSC 2015* (2015). doi:10.1109/PVSC.2015.7356174.
44. Simon, M. & Meyer, E. L. The effects of spectral evaluation of c-Si modules. *Progress in Photovoltaics: Research and Applications* (2011) doi:10.1002/pip.973.
45. Philipps, S. P. *et al.* Energy harvesting efficiency of III-V triple-junction concentrator solar cells under realistic spectral conditions. *Solar Energy Materials and Solar Cells* (2010) doi:10.1016/j.solmat.2010.01.010.
46. Reynolds, S. & Smirnov, V. Modelling Performance of Two- and Four-terminal Thin-film Silicon Tandem Solar Cells under Varying Spectral Conditions. in *Energy Procedia* (2015). doi:10.1016/j.egypro.2015.12.321.
47. Minemoto, T., Nagae, S. & Takakura, H. Impact of spectral irradiance distribution and temperature on the outdoor performance of amorphous Si photovoltaic modules. *Solar Energy Materials and Solar Cells* **91**, 919–923 (2007).
48. Ripalda, J. M., Chemisana, D., Llorens, J. M. & García, I. Location-Specific Spectral and Thermal Effects in Tracking and Fixed Tilt Photovoltaic Systems. *iScience* **23**, (2020).
49. Kinsey, G. S. *Preprint: Solar cell efficiency divergence due to operating spectrum variation.* <https://engrxiv.org/yfx9r/> (2020) doi:10.31224/osf.io/yfx9r.
50. Riedel-Lyngskar, N. *et al.* Spectral Albedo in Bifacial Photovoltaic Modeling: What can be learned from Onsite Measurements? *2021 IEEE 48th Photovoltaic Specialists Conference (PVSC)* 0942–0949 (2021) doi:10.1109/PVSC43889.2021.9519085.
51. Neves, G., Vilela, W., Pereira, E., Yamasoe, M. & Nofuentes, G. Spectral impact on PV in low-latitude sites: The case of southeastern Brazil. *Renewable Energy* **164**, 1306–1319 (2021).

52. Amillo, A. M. G., Huld, T., Vourlioti, P., Müller, R. & Norton, M. Application of satellite-based spectrally-resolved solar radiation data to PV performance studies. *Energies* (2015) doi:10.3390/en8053455.
53. Futscher, M. H. & Ehrler, B. Modeling the Performance Limitations and Prospects of Perovskite/Si Tandem Solar Cells under Realistic Operating Conditions. *ACS Energy Letters* (2017) doi:10.1021/acseenergylett.7b00596.
54. Louwen, A., de Waal, A. C., Schropp, R. E. I., Faaij, A. P. C. & van Sark, W. G. J. H. M. Comprehensive characterisation and analysis of PV module performance under real operating conditions. *Progress in Photovoltaics: Research and Applications* **25**, 218–232 (2017).
55. Braga, M., Rafael Do Nascimento, L. & Rüther, R. *Spectral Impacts on the Performance of mc-Si and New-Generation CdTe Photovoltaics in the Brazilian Northeast*.
56. Conde, L. A. *et al.* Spectral effects on the energy yield of various photovoltaic technologies in Lima (Peru). *Energy* **223**, 120034 (2021).
57. Braga, M., do Nascimento, L. R. & Rüther, R. Spectral modeling and spectral impacts on the performance of mc-Si and new generation CdTe photovoltaics in warm and sunny climates. *Solar Energy* **188**, 976–988 (2019).
58. Sirisamphanwong, C. & Ketjoy, N. Impact of spectral irradiance distribution on the outdoor performance of photovoltaic system under Thai climatic conditions. *Renewable Energy* **38**, 69–74 (2012).
59. Representative identification of spectra and environments (RISE) using k-means - Looney - 2021 - Progress in Photovoltaics: Research and Applications - Wiley Online Library. <https://onlinelibrary.wiley.com/doi/10.1002/pip.3358>.
60. Looney, E. E. *et al.* Representative identification of spectra and environments (RISE) using k-means. *Progress in Photovoltaics: Research and Applications* **29**, 200–211 (2021).
61. Braga, M., do Nascimento, L. R. & Ruther, R. Spectral Impacts on the Performance of mc-Si and New-Generation CdTe Photovoltaics in the Brazilian Northeast. *Conference Record of the IEEE Photovoltaic Specialists Conference* 1226–1231 (2019) doi:10.1109/PVSC40753.2019.8981152.
62. Magare, D. B. *et al.* Effect of seasonal spectral variations on performance of three different photovoltaic technologies in India. *International Journal of Energy and Environmental Engineering* **7**, (2016).
63. Riedel, N. *et al.* Direct Beam and Diffuse Spectral Irradiance Measurements in a Nordic Country Analyzed with the Average Photon Energy Parameter. *2018 IEEE 7th World Conference on Photovoltaic Energy Conversion, WCPEC 2018 - A Joint Conference of 45th IEEE PVSC, 28th PVSEC and 34th EU PVSEC* 2575–2580 (2018) doi:10.1109/PVSC.2018.8548240.
64. Rüther, R. & Livingstone, J. Seasonal variations in amorphous silicon solar module outputs and thin film characteristics. *Solar Energy Materials and Solar Cells* **36**, 29–43 (1995).
65. Rüther, R., Kleiss, G. & Reiche, K. Spectral effects on amorphous silicon solar module fill factors. *Solar Energy Materials and Solar Cells* **71**, 375–385 (2002).
66. PVPS Task, I. Climatic Rating of Photovoltaic Modules: Different Technologies for Various Operating Conditions PVPS Task 13 Performance, Operation and Reliability of Photovoltaic Systems.
67. PVPS Task, I. Climatic Rating of Photovoltaic Modules: Different Technologies for Various Operating Conditions PVPS Task 13 Performance, Operation and Reliability of Photovoltaic Systems.
68. IEC 61853-3:2018 | IEC Webstore | rural electrification, solar power, LVDC. <https://webstore.iec.ch/publication/26850>.

69. IEC 61853-4:2018 | IEC Webstore | rural electrification, solar power, LVDC. <https://webstore.iec.ch/publication/27908>.
70. Peters, I. M., Liu, H., Reindl, T. & Buonassisi, T. Global Prediction of Photovoltaic Field Performance Differences Using Open-Source Satellite Data. *Joule* **2**, 307–322 (2018).
71. Spectroradiometers | EKO Instruments. <https://eko-eu.com/products/solar-energy/spectroradiometers>.
72. Tatsiankou, V. *et al.* Extensive validation of solar spectral irradiance meters at the World Radiation Center. *Solar Energy* **166**, 80–89 (2018).
73. Tatsiankou, V., Hinzer, K., Schriemer, H., McVey-White, P. & Beal, R. Efficient, Real-Time Global Spectral and Broadband Irradiance Acquisition. *2018 IEEE 7th World Conference on Photovoltaic Energy Conversion, WCPEC 2018 - A Joint Conference of 45th IEEE PVSC, 28th PVSEC and 34th EU PVSEC* 2362–2365 (2018) doi:10.1109/PVSC.2018.8547671.
74. Gueymard, C. A. SMARTS2: a simple model of the atmospheric radiative transfer of sunshine: algorithms and performance assessment. *Report No. FSEC-PF-270-95* (1995).
75. Myers, D. R. & Gueymard, C. A. Description and availability of the SMARTS spectral model for photovoltaic applications. in *Organic Photovoltaics V* (2004). doi:10.1117/12.555943.
76. Myers, D. R., Emery, K. & Gueymard, C. Terrestrial solar spectral modeling tools and applications for photovoltaic devices. in *Conference Record of the IEEE Photovoltaic Specialists Conference* (2002). doi:10.1109/pvsc.2002.1190943.
77. Xie, Y. & Sengupta, M. A Fast All-sky Radiation Model for Solar applications with Narrowband Irradiances on Tilted surfaces (FARMS-NIT): Part I. The clear-sky model. *Solar Energy* (2018) doi:10.1016/j.solener.2018.09.056.
78. Xie, Y., Sengupta, M. & Wang, C. A Fast All-sky Radiation Model for Solar applications with Narrowband Irradiances on Tilted surfaces (FARMS-NIT): Part II. The cloudy-sky model. *Solar Energy* (2019) doi:10.1016/j.solener.2019.06.058.
79. Kinsey, G. S., Stone, K., Brown, J. & Garboushian, V. Energy prediction of Amonix CPV solar power plants. *Progress in Photovoltaics: Research and Applications* **19**, (2011).
80. Kinsey, G. S. Weighing the merits of solar power plants using concentration photovoltaics - PV Tech. *PV Tech* <https://www.pv-tech.org/technical-papers/weighing-the-merits-of-solar-power-plants-using-concentration-photovoltaics/> (2012).
81. Kinsey, G. S. *et al.* Advancing efficiency and scale in CPV Arrays. *IEEE Journal of Photovoltaics* **3**, (2013).
82. Yamasoe, M. A., Artaxo, P., Miguel, A. H. & Allen, A. G. Chemical composition of aerosol particles from direct emissions of vegetation fires in the Amazon Basin: Water-soluble species and trace elements. *Atmospheric Environment* **34**, 1641–1653 (2000).
83. JD Haigh, AR Winning, R Toumi & JW Harder. An influence of solar spectral variations on radiative forcing of climate. *Nature* **467**, 696–699 (2010).
84. Foote, E. Circumstances Affecting the Heat of the Sun's Rays. *The American Journal of Science and Arts, Art. XXXI* 382 [https://books.google.co.uk/books?id=fjtSAQAAMAAJ&lpg=PA382&dq="Circumstances Affecting the Heat of the Sun's Rays" foote&pg=PA382](https://books.google.co.uk/books?id=fjtSAQAAMAAJ&lpg=PA382&dq=) (1856).
85. Green, M. A. *et al.* Solar cell efficiency tables (Version 53). *Progress in Photovoltaics: Research and Applications* (2019) doi:10.1002/pip.3102.

86. Green, M. A. *et al.* Solar cell efficiency tables (version 50). *Progress in Photovoltaics: Research and Applications* (2017) doi:10.1002/pip.2909.
87. Green, M. A., Emery, K., Hishikawa, Y., Warta, W. & Dunlop, E. D. Solar cell efficiency tables (Version 45). *Progress in Photovoltaics: Research and Applications* (2015) doi:10.1002/pip.2573.
88. Green, M. A. *et al.* Solar cell efficiency tables (Version 55). *Progress in Photovoltaics: Research and Applications* (2020) doi:10.1002/pip.3228.
89. Green, M. A. *et al.* Solar cell efficiency tables (version 56). *Progress in Photovoltaics: Research and Applications* (2020) doi:10.1002/pip.3303.
90. Green, M. A., Emery, K., Hishikawa, Y., Warta, W. & Dunlop, E. D. Solar cell efficiency tables (version 42). *Progress in Photovoltaics: Research and Applications* (2013) doi:10.1002/pip.2404.
91. EU PVSEC Proceedings - Impact of High Light Transmission EVA-Based Encapsulant on the Performance of PV Modules. <https://www.eupvsec-proceedings.com/proceedings?paper=18549>.
92. Kinsey, G. S. 2021 Photovoltaic Reliability Workshop Poster Session D, "Solar cell efficiencies under operating spectra" D-2 February 25, 2021 - YouTube. <https://www.youtube.com/watch?v=Uctmjh06KKQ&t=3240s> (2021).
93. Kleiss, G. & Bücher, K. The Need for an International Energy Rating Concept for Photovoltaic Modules. *12th EC Photovoltaic Solar Energy Conference* 299 https://www.researchgate.net/publication/282694733_The_need_for_an_International_Energy_Rating_Concept_for_Photovoltaic_Modules (1994).
94. Raicu, A., Heidler, K., Kleiss, G. & Bücher, K. Realistic reporting conditions -RRC- for site-dependent energy rating of PV devices. in *11th European Photovoltaic Solar Energy Conference* (eds. Communities, C. of the E. & Guimarães, L. (Leopoldo)) 1323–1326 (Harwood Academic, 1993).
95. IEC 60904-7. *IEC 60904-7 Edition 3.0 Part 7: Computation of the spectral mismatch correction for measurements of photovoltaic devices*. International Electrotechnical Commission (2008).
96. Renewables Won't Save Us If The Electric Grid Is Not Ready. <https://www.forbes.com/sites/davidblackmon/2020/09/30/renewables-wont-save-us-if-the-electric-grid-is-not-ready/?sh=2340043c7abf>.
97. Hangzhou Air Quality Index (AQI) and China Air Pollution | AirVisual. <https://www.iqair.com/us/china/zhejiang/hangzhou>.
98. Ito, M., Kato, K., Komoto, K., Kichimi, T. & Kurokawa, K. Analysis of transmission losses of very large-scale photovoltaic power generation systems (VLS-PV) in world desert. *Conference Record of the IEEE Photovoltaic Specialists Conference* 1706–1709 (2005) doi:10.1109/PVSC.2005.1488477.
99. Wild, M. Global Dimming and Brightening. *Global Environmental Change* 39–47 (2014) doi:10.1007/978-94-007-5784-4_27.
100. Kipp & Zonen. *Solar Irradiance Monitoring in Solar Energy Projects*. <https://www.kippzonen.com/Download/810/Brochure-Solar-Irradiance-Monitoring-in-Solar-Energy-Projects>.
101. Built solar assets are 'chronically underperforming' and modules degrading faster than expected, research finds - PV Tech. <https://www.pv-tech.org/built-solar-assets-are-chronically-underperforming-and-modules-degrading-faster-than-expected-research-finds/>.
102. IRENA. Electricity storage and renewables: Costs and markets to 2030. </publications/2017/Oct/Electricity-storage-and-renewables-costs-and-markets>.

103. NREL. Electrification Futures Study: A Technical Evaluation of the Impacts of an Electrified U.S. Energy System | Energy Analysis | NREL. <https://www.nrel.gov/analysis/electrification-futures.html>.
104. California invested heavily in solar power. Now there's so much that other states are sometimes paid to take it - Los Angeles Times. <https://www.latimes.com/projects/la-fi-electricity-solar/>.
105. Herscher, R. Texas Electricity Bills Skyrocket Due To Winter Storm : Live Updates: Winter Storms 2021 : NPR. *NPR* <https://www.npr.org/sections/live-updates-winter-storms-2021/2021/02/21/969912613/after-days-of-mass-outages-some-texas-residents-now-face-huge-electric-bills> (2021).
106. Penney, V. How Texas' Power Generation Failed During the Storm, in Charts - The New York Times. *New York Times* <https://www.nytimes.com/interactive/2021/02/19/climate/texas-storm-power-generation-charts.html> (2021).
107. SunPower. SunPower product performance. *Products* <https://us.sunpower.com/products/solar-panels> (2020).
108. Driesse, A. & Stein, J. S. Global normal spectral irradiance in Albuquerque: a one-year open dataset for PV research. *Sandia National Laboratory, SAND2020-12693* <https://pvpmc.sandia.gov/modeling-steps/1-weather-design-inputs/irradiance-and-insolation-2/irradiance-data-sources-for-performance-modeling/spectral-irradiance-data-from-albuquerque/> (2020).
109. Flynn, C., Mendoza, A. & Shi, Y. Shortwave Array Spectroradiometer-Hemispheric (SASHEVIS). 2016-05-16 to 2017-11-01, ARM Mobile Facility (ASI) Ascension Island, South Atlantic Ocean; AMF1 (M1). *Atmospheric Radiation Measurement (ARM) user facility* <http://dx.doi.org/10.5439/1150262> doi:10.5439/1150262 10.5439/1150263.
110. Flynn, C., Mendoza, A. & Shi, Y. Shortwave Array Spectroradiometer-Hemispheric (SASHEVIS & SASHENIR). 2012-07-21 to 2013-06-21, ARM Mobile Facility (PVC) Highland Center, Cape Cod MA; AMF1 (M1). *Atmospheric Radiation Measurement (ARM) user facility* <http://dx.doi.org/10.5439/1150263> doi:10.5439/1150263, 10.5439/1150262.
111. Flynn, C., Mendoza, A. & Shi, Y. Shortwave Array Spectroradiometer-Hemispheric (SASHEVIS & SASHENIR). 2018-10-06 to 2019-04-30, ARM Mobile Facility (COR) Córdoba, Argentina. *Atmospheric Radiation Measurement (ARM) user facility* <http://dx.doi.org/10.5439/1150262> doi:10.5439/1150262, 10.5439/1150263.
112. MIDC: University of Oregon (SRML). <https://midcdmz.nrel.gov/apps/sitehome.pl?site=UOSMRL>.
113. NIST Photovoltaic Data. <https://pvdata.nist.gov/>.
114. MIDC: NREL Solar Radiation Research Laboratory (BMS). <https://midcdmz.nrel.gov/apps/sitehome.pl?site=BMS>.
115. Flynn, C., Mendoza, A. & Shi, Y. Shortwave Array Spectroradiometer-Hemispheric (SASHEVIS & SASHENIR). 2013-01-01 to 2016-12-31, Southern Great Plains (SGP) Central Facility, Lamont, OK (C1). *Atmospheric Radiation Measurement (ARM) user facility* <http://dx.doi.org/10.5439/1150262> doi:10.5439/1150262, 10.5439/1150263.
116. Flynn, C., Mendoza, A. & Shi, Y. Shortwave Array Spectroradiometer-Hemispheric (SASHEVIS & SASHENIR). 2014-01-01 to 2015-12-01, ARM Mobile Facility (MAO) Manacapuru, Amazonas, Brazil. *Atmospheric Radiation Measurement (ARM) user facility* <http://dx.doi.org/10.5439/1150262> doi:10.5439/1150262, 10.5439/1150263.
117. Kurtz, S. *et al.* Analysis of Photovoltaic System Energy Performance Evaluation Method. (2013).

118. WISER | Spectroradiometer | EKO Instruments. <https://eko-eu.com/products/solar-energy/spectroradiometers/wiser-i-spectroradiometer>.
119. SolarSIM-G | Spectrafy. <https://www.spectrafy.com/products/solarsim-g>.
120. Pavanello, D. *et al.* Results of the IX International Spectroradiometer Intercomparison and impact on precise measurements of new photovoltaic technologies. *Progress in Photovoltaics: Research and Applications* **29**, 109–123 (2021).
121. Schinke, C. *et al.* Calibrating spectrometers for measurements of the spectral irradiance caused by solar radiation. *Metrologia* **57**, 065027 (2020).
122. Kinsey, G. S. *et al.* Concentrator multifunction solar cell characteristics under variable intensity and temperature. *Progress in Photovoltaics: Research and Applications* **16**, (2008).
123. NREL. NSRDB Data Viewer. *National Renewable Energy Laboratory (NREL)* <https://maps.nrel.gov/nsrdb-viewer/>.
124. Sengupta, M. *et al.* The National Solar Radiation Data Base (NSRDB). *Renewable and Sustainable Energy Reviews* (2018) doi:10.1016/j.rser.2018.03.003.

AUTHOR AFFILIATIONS:

-
- ¹ Zuva Energy, New York, USA. Email: geoffreykinsey@zuvaenergy.com
 - ² Department of Photonics Engineering, Technical University of Denmark, Roskilde, Denmark
 - ³ Centro de Investigaciones Energéticas, Medioambientales y Tecnológicas (CIEMAT), Madrid, Spain
 - ⁴ National Renewable Energy Laboratory, Golden, USA
 - ⁵ Laboratório Fotovoltaica/UFSC, Universidade Federal de Santa Catarina, Florianópolis, Brazil
 - ⁶ Key Laboratory of Solar Energy Utilization & Energy Saving Technology of Zhejiang Province, China
 - ⁷ Departamento de Física, Universidad de Santiago de Chile, Santiago, Chile
 - ⁸ Commonwealth Scientific and Industrial Research Organisation (CSIRO) Energy, Newcastle, Australia
 - ⁹ FOSS Research Centre for Sustainable Energy, University of Cyprus, Cyprus
 - ¹⁰ Florida Solar Energy Center (FSEC), Cocoa, USA
 - ¹¹ MBR Solar Park, Dubai, UAE
 - ¹² School of Renewable Energy and Smart Grid Technology, Naresuan University, Thailand
 - ¹³ Universidad de Huelva, Huelva, Spain
 - ¹⁴ Institute for Renewable Energy, Eurac Research, Bolzano, Italy
 - ¹⁵ Council for Scientific and Industrial Research (CSIR), Pretoria, South Africa
 - ¹⁶ Department of Electrical and Electronic Engineering, Ritsumeikan University, Kusatsu, Japan
 - ¹⁷ Center for Energy, Austrian Institute of Technology - AIT, Vienna, Austria
 - ¹⁸ Brazilian National Institute for Space Research (Instituto Nacional de Pesquisas Espaciais - INPE)
 - ¹⁹ IDEA Research Group, Center for Advanced Studies in Earth Science, Energy and Environment (CEACTEMA), University of Jaén, Jaén, Spain
 - ²⁰ University of Agder, Faculty of Engineering and Sciences, Grimstad, Norway
 - ²¹ Natural Resources Canada, Ottawa, Canada
 - ²² Solar Energy Research Institute of Singapore (SERIS), National University of Singapore (NUS), Singapore
 - ²³ Utrecht University, Copernicus Institute of Sustainable Development, Utrecht, Netherlands
 - ²⁴ Departamento de Ciencias, Sección Física, Pontificia Universidad Católica Del Perú, Lima, Perú
 - ²⁵ Sandia National Laboratories, Albuquerque, USA
 - ²⁶ Helmholtz-Zentrum Berlin, Berlin, Germany
 - ²⁷ Key Laboratory of Middle Atmosphere and Global Environment Observation (LAGEO), Institute of Atmospheric Physics, Chinese Academy of Sciences, Beijing, China.
 - ²⁸ Instituto de Astronomia, Geofísica e Ciências Atmosféricas, Universidade de São Paulo, São Paulo, Brazil